Pageoph, Vol. 114 (1976), Birkhäuser Verlag, Basel

Theory of Earthquakes – IV. General Implications for Earthquake Prediction

By B. T. BRADY[1])

Abstract – The scale invariant inclusion theory of failure is applied to the general problem of precursors that precede failure. A precursor is defined to be an effect produced within a physical system which indicates that the process leading to failure of the system has begun. Precursors are grouped into three classes. *Class I* precursors refer to long-term indicators of impending failure. These may include v_p/v_s, long-term tilt, and crustal uplift anomalies observed to precede some major shallow earthquakes by a *few years*. *Class II* precursors refer to short-term indicators of failure and include: S-bend tilt, electromagnetic radiation, radon emanations, and seismicity changes that have been reported to precede major earthquakes by a *few hours*. *Class III* precursors refer to *very* short-term phenomena such as long-period (strain) waves, *rapid* changes in surface ground tilts, and seismicity increase in the hypocentral region that are predicted by the inclusion theory to precede major shallow earthquakes by a *few seconds*.

The physical processes that occur within the inclusion zone of an impending failure that indirectly produce the class II precursors are used with the scale invariant properties of failure to show that their time duration is a direct measure of the average length of the cracks that comprise the inclusion zone. This result is used to derive the precursor time–'fault' length relationship that has been observed to hold for class I precursors of shallow earthquakes, mine failures, and laboratory size failures of rock. The physical model proposed for producing class I, class II, and indirectly, the class III precursors leads to six results when both the Utsu relationship between aftershock area and earthquake magnitude and the Gutenberg–Richter energy–magnitude relationship are satisfied. (1) The seismic efficiency factor for failures satisfying the constraints of the inclusion theory is approximately 0.40%. (2) The energy radiated by aftershocks will be at least 1.0% of the energy radiated by the mainshock. (3) An upper limiting magnitude of any aftershock in the aftershock sequence is $M - 1.6$, where M is the mainshock magnitude. (4) The time durations of all three precursor classes are shown to be shortened (or lengthened) by a factor inversely proportional to the rate of increase (or decrease) of the far-field stresses during the time duration of the precursor. Changes in far-field stresses, such as might occur to tidal effects, are shown to be of particular importance in initiating class II precursors, and it is shown that tidal stresses provide a mechanism for triggering large earthquakes ($M \geq 6.0$) in regions that are at the point of incipient failure. Thus, class II precursors may give the appearance of being independent of magnitude for large earthquakes. (5) When fluids are present in the focal volume of the mainshock, the predicted magnitude, calculated by class I precursors, will always be larger than the observed magnitude. (6) Seismic events that produce the inclusion zone of the impending mainshock will not be followed by aftershocks. These events are predicted to be characterized by anomalously long rupture lengths.

The inclusion theory is shown to provide a physical basis for criteria required to predict failure. The implications of the inclusion theory to the problem of earthquake prediction are discussed. The theory is applied to existing earthquake-prone regions.

[1]) Physicist, U.S. Department of the Interior, BuMines, Denver Mining Research Center, Denver, Colorado, 80225 USA.

Introduction

A precursor is defined in this article to be an effect produced within a physical system which indicates that the process leading to failure of the system has begun. Precursors of failure will be grouped into three distinct classes. *Class I* precursors refer to the long-term indicators of impending failure and may include v_p/v_s, long-term tilt, *b*-value, and crustal uplift anomalies that are often observed to precede major shallow earthquakes by a few years [3, 13, 14, 19, 28, 29, 34, 35, 39, 43].[2] A physical model that explains many of the essential features of this precursor class has been described elsewhere [6, 7]. *Class II* precursors will be defined to represent short-term indicators of failure. For example, there is some evidence that tilt changes, in addition to the tilt anomaly of the class I type, develop several hours prior to major shallow earthquakes ($M \sim 7.0$). These tilt changes are termed S-bend tilt and are characterized by *two* reversals in the tilt direction in the vicinity of the earthquake epicenter shortly ($\sim$few hours) before the mainshock [28, 29]. Similarly, in addition to S-bend tilt, there are other class II precursors that have been reported. These include anomalous short-term vertical and horizontal crustal displacements, electrical and magnetic effects, change in water level, and in some instances, increased seismicity in the hypocentral region of the mainshock [16, 19, 28, 29, 33, 47]. There is experimental and theoretical evidence suggesting that class II precursors may be causally related to physical processes that occur in the hypocentral region prior to the mainshock [6, 7]. *Class III* precursors will be defined to represent *very* short-term phenomena of impending failure and include phenomena such as long-period (strain) waves, *rapid* changes in surface ground tilts, and seismicity increase in the hypocentral region predicted by the inclusion theory to precede major shallow earthquakes by a few seconds [10].

The study of precursors of failure and, in particular, class II precursors, their general implications for earthquake prediction, and their importance to the understanding of the physical processes involved in the preparation of a region for failure forms the subject matter of this article. The article is divided into two sections. The first section is concerned with the mathematical development of the inclusion theory. A problem of special importance examined in this section is determining the criteria for recognizing that a region has approached a condition that it will experience a failure. The second section is concerned with the application of these criteria to existing shallow earthquake zones in the earth.

Physics of failure

In order to understand the physical processes that produce the precursors of failure, a detailed physical model of the failure process in an impending failure zone

[2]) Numbers in brackets refer to references listed at the end of this article.

is required. This subject is examined in this section. For convenience, the reader is referred to Appendix A for a glossary of symbols and terms used in the article.

Class I precursors of failure: their physical basis

Four distinct phases have been postulated and experimentally demonstrated to precede fault growth in rock on a small scale (laboratory) [6, 9]. These behavioral phases have been shown to be scale invariant over a wide range of sample sizes and are, therefore, *fully* applicable to the earthquake process [7, 8, 11, 12]. These phases are also applicable to describing failures that occur within lock point regions along preexisting fault zones (Figs. 1d, 2). The characteristics of these phases are clarified and summarized here as the basis for later arguments.

Dilatant phase: Cracks form within the rock mass in response to the applied far-field stresses. The far-field stresses refer to the stresses that exist within the rock mass

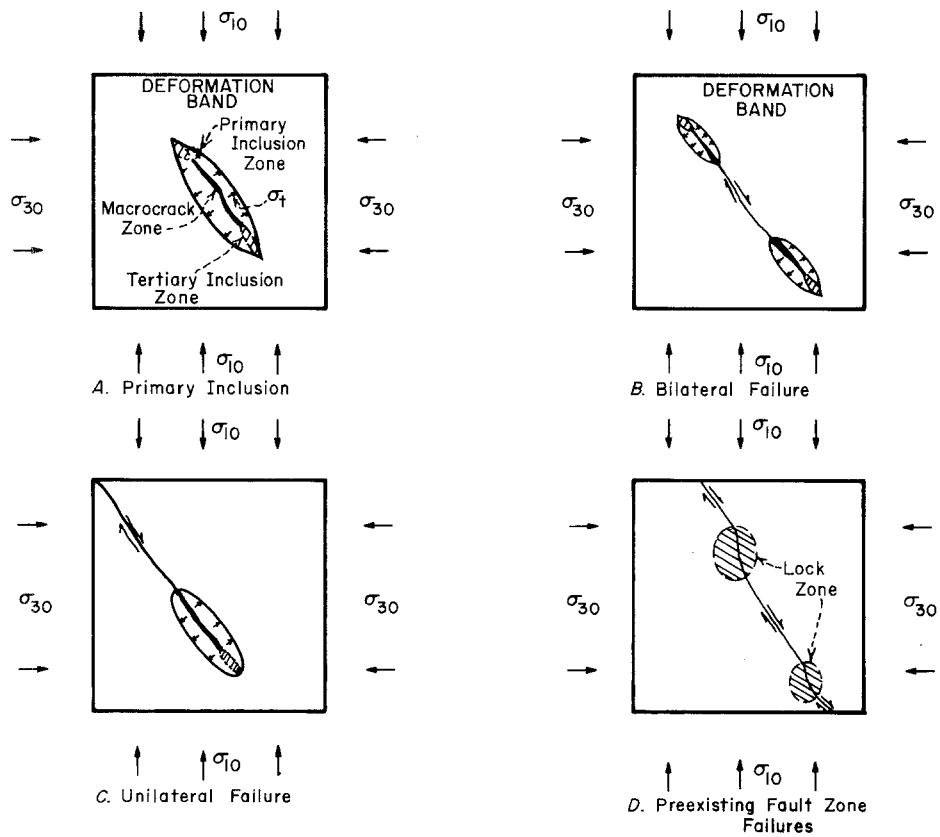

Figure 1
Classification scheme for shear failure illustrating the formation of the primary inclusion zone within the deformation band (A). Bilateral and unilateral failure classes are shown diagramatically in B–C. Failure along a preexisting fault zone is illustrated in D.

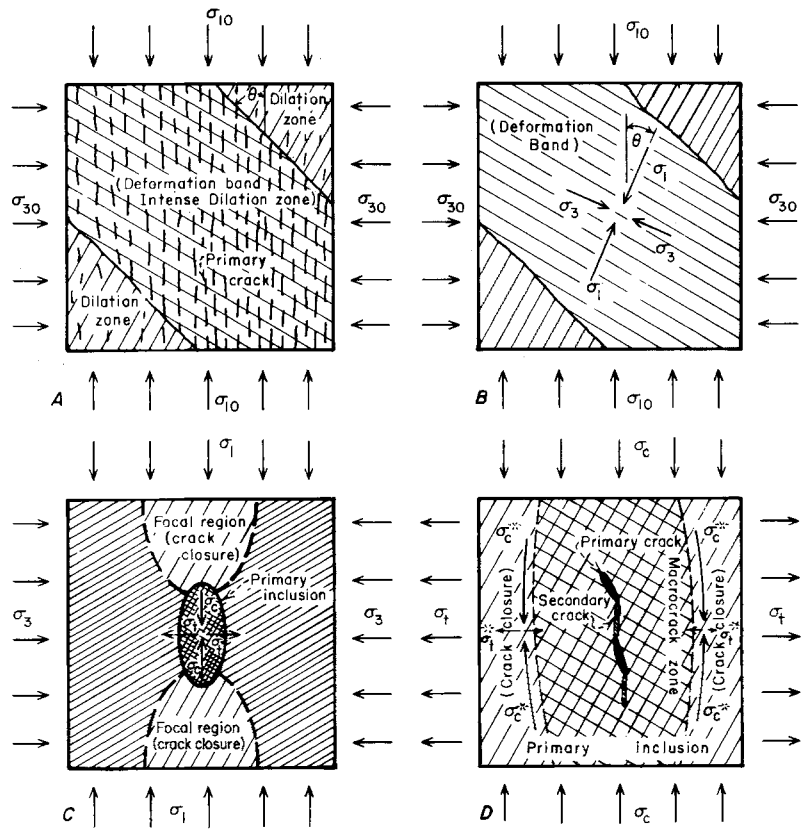

Figure 2
Sequence of macrocrack growth prior to failure. This figure illustrates the formation of the primary inclusion zone within the deformation band (anomalous region) (A–C). The formation of the secondary cracks within the primary inclusion zone and their coalescence with the primary cracks to form a macrocrack is illustrated in D.

at a distance far-removed from the dilatant zone (hereafter referred to as the *anomalous* region). In Figs. 1 and 2, the maximum and minimum far-field principal applied stresses are denoted by σ_{10} and σ_{30}. The intermediate principal stress, σ_{20}, is assumed equal to σ_{30} for the sake of argument. The *dilatant* or *anomalous* phase begins at a maximum far-field principal stress whose magnitude is *usually* well below the ultimate strength of the rock mass. This phase culminates in the formation of crack clusters [deformation band(s) (Fig. 2a)] within the anomalous volume when the rock mass is within a few percent of its ultimate strength. The deformation band(s) behaves physically as a low modulus elastic inclusion(s) that is embedded within a host material (dilatant and uncracked volume) of higher elastic modulus. This elastic contrast produces a rotation, θ, and change in magnitude ($\sigma_{10} \rightarrow \sigma_1, \sigma_{30} \rightarrow \sigma_3$) of the principal stresses both within and in the vicinity of the deformation band. The

magnitude of σ_3 decreases in compression within the deformation band as the deformation band softens. The amount of stress axis rotation and the change in the stress values depend on the relative elastic contrast between the deformation band and the surrounding material [6]. An example and brief discussion of this behavioral phase is presented in Appendix B.

Inclusion phase: Additional cracks will develop in response to local stress conditions existing within the deformation band as the applied far-field stresses (σ_{10}, σ_{30}) continue to increase. Cracks may also develop along the boundaries of the deformation band due to stress concentrating effects of the deformation band and as the deformation band continues to soften in response to continuing crack growth within the band. At a point in time before failure, an *inclusion zone, termed the primary inclusion zone* will develop *within* the deformation band (Figs. 1, 2c). In the context of this article, the primary inclusion zone represents a region of highly concentrated dilatancy that forms at a time before failure that is dependent only on the size (magnitude) of the failure that is to follow and the time rate of change of the far-field applied stresses [6, 7].

Once the primary inclusion zone has formed, compressive (σ_c) and tensile (σ_t) stresses are induced within the zone parallel to and normal to, respectively, the eventual direction of fault growth (Fig. 2c). These stresses are a result of the elastic contrast between the primary inclusion zone and the surrounding material. It is important to observe that the primary inclusion zone exists, or begins to evolve, *only when the least principal stress within the deformation band in the vicinity of where the primary inclusion zone will form changes from compression to tension.* The formation of the primary inclusion zone causes the *local* principal stress difference σ_d ($= \sigma_1 - \sigma_3$) to decrease in the focal region of the primary inclusion, that is, the region into which the primary inclusion will grow at the instant of failure (Figs. 1, 2c). Class I precursors, such as tilt and seismicity rate, will begin to exhibit deviations from their 'normal' pre-earthquake values as the primary inclusion zone forms. The seismic velocities v_p and v_s will decrease for seismic ray paths that pass through the primary inclusion zone. There will be *no* change for ray paths passing only through the focal region. Note also that b-values will decrease from their 'normal' background level for the seismic events that form the deformation band. The physical cause for the b-value decrease is that the local least principal stress decreases during the formation of the deformation band. Thus, some of the energy that normally would have been dissipated by frictional sliding for these events will now be available to power the growth of these events into their respective focal regions where the value of the least principal stress is σ_3 ($\sigma_3 < \sigma_{30}$). Hence, the effective magnitudes of the seismic events will tend to increase as the deformation band softens, that is, as σ_3 decreases in compression. The largest b-value decreases will be for the events that form the primary inclusion zone of the forthcoming mainshock since the value of σ_3 in the vicinity of where the primary inclusion zone will form is approximately zero.

Closure phase: Crack closure occurs in the focal region in response to the decrease

in magnitude of the *local* shear stress and the corresponding increase (*in compression*) of the least principal stress (σ_3). The seismically determined stress axes that produce crack closure will be rotated 90° from the stress axes that produced the cracks that comprise the anomalous volume and the primary inclusion zone. Thus, the strain energy density increases throughout the focal region and approaches its *maximum possible value* when all cracks that formed during the dilatant phase are closed. Consequently, the focal region *will* become elastically stiffer than its surroundings and, as such, will behave physically as a *stress guide* for the direction of fault growth during the growth phase of the failure. *Therefore, focusing of the strain energy, some of which will be released during the mainshock, is predicted to occur in a direction parallel to the rupture propagation direction.*

Shortly before failure, when the focal region of the primary inclusion zone has become elastically stiffer than the surrounding anomalous volume, the stress differ ence will increase outside the focal region in the direction of eventual fault growth. Thus, increased seismicity is predicted by the model to occur outside the focal region prior to the mainshock. The seismically determined stress axes of these seismic events will exhibit an orientation similar, *though not identical*, to the stresses that produced cracks during the dilatant phase within the anomalous zone.

It is not a necessary and sufficient condition for cracks to be physically present in the focal region of the primary inclusion to produce failure. The presence of the primary inclusion zone produces both a reversal in the local principal stress difference and an increase in the mean pressure in the focal region. These two conditions give rise to an increasing value of σ_t within the primary inclusion zone as this zone evolves toward its final pre-failure state. *Thus, v_p, v_s and/or v_p/v_s anomalies need not exist within the focal region prior to the failure.* Therefore, when the focal region of the impending failure is 'dry', that is, when effects due to fluid diffusion away from the primary inclusion zone can be neglected, the seismic velocities v_p and v_s will both increase during the closure phase for ray paths passing through the focal region. There will be no increase in v_p and v_s from their 'normal' background values during the formation of the primary inclusion zone. However, when the focal region is wet, fluid diffusion away from the primary inclusion zone (in response to crack closure) may produce small fractures within the focal region, causing both v_p and v_s to locally decrease for ray paths through the focal region. These velocities will recover to their pre-dilatant values only when the closure front has passed.

Just prior to failure, the tensile stress, σ_t, in the interior of the primary inclusion approaches its maximum possible value when all cracks in the focal region have closed. If the ratio of the applied stresses (σ_1 and σ_3), σ_1/σ_3, is sufficiently small [(≤ 0.10)], secondary cracks (Fig. 2d) (termed *primary* foreshocks of the impending mainshock) will form in the primary inclusion zone. Coalescence of the primary and secondary crack occurs and macrocrack growth begins within the macrocrack zone (Figs. 2c,d). It is important to observe that *both* the shear stress and shear strain will decrease within the focal region prior to the mainshock, that is, during the class I

precursor phase. Similarly, both the mean pressure and volumetric strain will increase during this phase. In addition, both the shear stress and strain will increase within the focal region just prior to the mainshock in response to crack growth within the primary inclusion zone. This predicted behavior is in marked distinction from other 'dry' failure models [44, 48] where the shear strain increases as the shear stress decreases prior to failure.

Class II precursors of failure: their physical basis

The scale invariant inclusion theory has been used successfully to explain class I precursors, such as anomalous tilt and seismicity to mention a few, observed to occur a few years prior to major shallow earthquakes [7, 28, 29]. This theory also provides a physical basis for class II precursors, such as S-bend tilt, and several results of particular physical importance follow.

S-bend tilt. Figure 2d illustrates the formation of secondary cracks in response to an increasing magnitude of the tensile stress, σ_t, within the primary inclusion zone as the focal region of the primary inclusion begins to store strain energy. The secondary cracks lead to the formation of the macrocrack (macrocrack zone, Fig. 2d) by their coalescence with previously formed (primary) cracks whose lengths are comparable with the secondary cracks. Finite element modeling of this problem [8] has shown that the compressive stress, σ_c^*, increases along the boundary of the macrocrack zone as the macrocrack zone 'softens' in response to the generation of the cracks within the secondary inclusion zones that *will lead* to the formation of the secondary cracks. Thus, as the relative elastic contrast increases between the macrocrack zone and its surroundings, the local values of the stress difference and the mean pressure decrease and increase, respectively. Hence, cracks that formed earlier within the primary inclusion zone outside the macrocrack zone begin to close as the secondary inclusion zones that are contained within the macrocrack zone (Fig. 2d) evolve to their respective failure initiation points. Therefore, the thickness, or equivalently, the aspect ratio of the primary inclusion zone, defined as the zone that contains open cracks, must decrease as failure becomes imminent.

Figure 3 illustrates the fault-primary inclusion zones, the focal region of the primary inclusion zone, and the idealized behavior of a tiltmeter located on the surface above the focal region. The physical situation depicted in Fig. 3 would be that of a thrust fault earthquake-type geometry. Similar, though not as pronounced, tilt behavior will also be observed for a strike-slip fault earthquake type geometry [7]. The tiltmeter will exhibit the following sequence of events in response to physical processes occurring within the focal region and the primary inclusion zone prior to the failure. (1) Tilting is in a direction away from the primary inclusion zone as this zone evolves in response to the applied principal stress within the deformation band. This time interval will be evidenced by decreasing v_p/v_s values within the primary inclusion zone and other reported precursors such as seismicity and stress axis

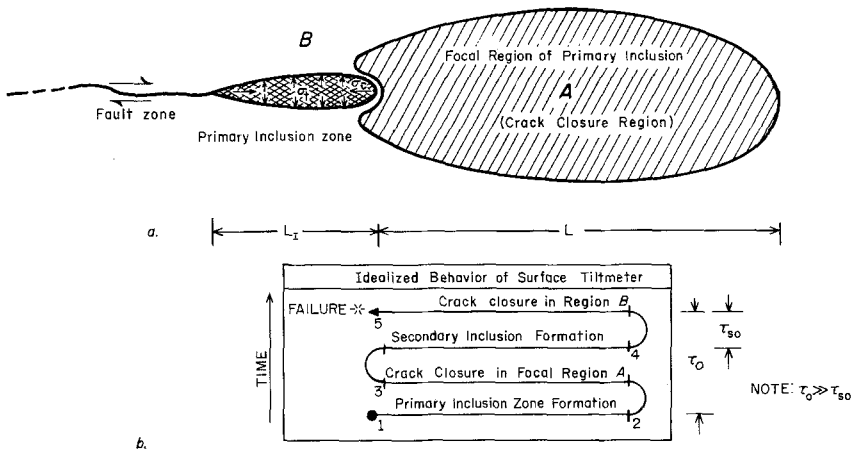

Figure 3
Fault zone—primary inclusion zone—focal region idealization of a thrust-fault geometry (a) and the idealized behavior of a hypothetical tiltmeter location on the surface above the focal region (b).

rotation within the focal region of the impending failure [7]. (2) Crack closure in the focal region of the primary inclusion will eventually dominate the deformation, causing a reversal in the tilt direction. Recovery of v_p/v_s *may occur* in the focal region, and other class I precursors, such as tilt, will return to their 'normal' predilatant values during this time interval. (3) Crack growth within the secondary inclusion zones that are themselves contained within the primary inclusion zone (macrocrack zone, Fig. 2d) eventually leads to the formation of the secondary cracks. Crack growth within the secondary inclusion zone produces tilting in a direction away from the primary inclusion zone. Note that the increased stress levels in the focal region of the primary inclusion may produce 'overshoot' of v_p/v_s above its pre-dilatant level; that is, its value prior to the formation of the primary inclusion zone, as additional cracks that were present prior to the anomalous phase close. (4) As cracks continue to form within the macrocrack zone, the stresses σ_c^* and σ_t^* increase and decrease, respectively, causing the closure of cracks outside the macrocrack zone. This closure will produce a reversal in the tilt direction. As these cracks close, the elastic contrast between the macrocrack zone and its surroundings approaches a maximum. The tensile stress in the primary inclusion zone, the stress concentration within its focal region, and the shear stress along the fault zone all approach their maximum pre-failure values. When the stress conditions within the primary inclusion zone are favorable to produce secondary crack growth, that is, those cracks that will coalesce with the primary cracks in the macrocrack zone, the failure must occur at this point in time as the principal stress difference within the focal region of the primary inclusion begins to increase during the class II precursor time [7]. Note that the predicted tilt direction will be toward the epicentral region just prior to the mainshock. Note also that this model predicts that the time duration of S-bend tilt

is a direct measure of the length of the secondary cracks that comprise the macrocrack zone. This time duration will also provide a direct measure of the average length of the cracks that initially formed the primary inclusion zone. In addition, the lengths of the secondary cracks are, in turn, directly related to the size (magnitude) of the failure that will be produced.

Other class II precursors. Other short-term precursors resulting from the physical processes that occur in the primary inclusion of the impending failure are also predicted to develop during the time duration of the S-bend tilt phase. For example, when the impending failure will be of a thrust-like geometry, these precursors will include the following phenomena. (1) The regional uplift displacement rate above the primary inclusion will increase in response to crack formation within the secondary inclusion zone during the early phases of S-bend tilt. The rate of uplift will begin to decrease in response to crack closure within the volume outside the macrocrack zone during the latter portions of the S-bend tilt phase. Thus, regional subsidence may occur above the primary inclusion zone just prior to the mainshock. Similarly, the rate of regional subsidence above the focal region of the primary inclusion will increase during the S-bend tilt phase in response to the increased stress levels during this phase. (2) Seismic velocities will increase as cracks close within the volume outside the macrocrack zone. (3) Seismicity will increase within the macrocrack zone as cracks form within the macrocrack zone. The energy released by this process is shown shortly to be at least five orders of magnitude less than the energy that will be released during the mainshock.

Direct field observations of some of these predicted precursors have been reported [19, 28, 29, 36]. For example, MATUZAWA [36] has reported evidence of rapid elevation changes a few minutes prior to the 1923 Kanto earthquake. Increased radon content shortly before earthquakes has been detected in wells far removed from the hypocentral region of impending large earthquakes [19]. Increased stress in these regions, resulting from crack growth within the macrocrack zone, may be responsible for this effect, thus suggesting that radon emission and increased stress levels prior to earthquakes are positive correlated quantities. Electromagnetic phenomena, if conditions favoring their existence are present [7], that may be stress induced have been reported to precede major earthquakes. Anomalous animal behavior prior to these earthquakes may also be a result of these same stress-induced electromagnetic effects. Such anomalies are consistent within the framework of the inclusion theory [7].

Class III precursors of failure: their physical basis

The inclusion theory rests on the postulate that failure occurs when all cracks in the focal region of the primary inclusion are closed, or equivalently, when the strain energy density throughout the focal region is a maximum. At this point in time, the physical contrast between the primary inclusion and its focal region becomes a maximum. The tension stress within the primary inclusion and the strain energy

density throughout its focal region reach a maximum just prior to the initiation of the mainshock. Crack growth occurs within the secondary inclusion zones, leading to the formation of secondary cracks, coalescence of these secondary cracks with the primary cracks occurs, and the macrocrack forms within the primary inclusion zone. This sequence of events marks the termination of the class II precursor stage. Growth of the macrocrack, or alternatively, the initiation of the mainshock sequence, begins at this point in time.

Growth of the macrocrack into *its* focal region, termed the tertiary inclusion zone (Fig. 4), will be evidenced by a decrease in the magnitude of the tensile stress within the primary inclusion to a value, say σ_t, that is below its maximum pre-failure value σ_{t0}. Closure of the macrocrack in the immediate vicinity of the fault zone will

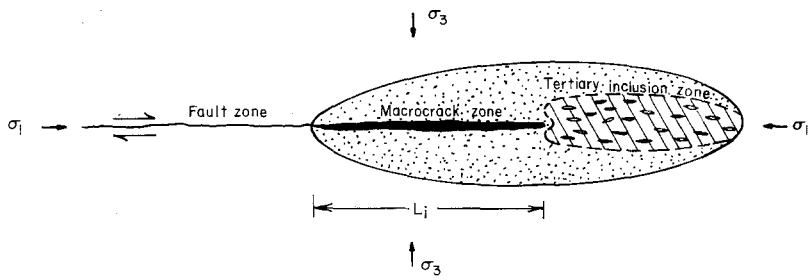

Figure 4
Illustration of the tertiary inclusion zone within the primary inclusion zone.

occur as the normal stress at the fault-primary inclusion zone boundary increases as the tensile stress within the primary inclusion zone increases. In the inclusion theory, failure can continue only when the tension stress within the primary inclusion equals its maximum pre-failure value (σ_{t0}), that is, the tensile stress that exists in the immediate vicinity of the macrocrack tip (tertiary inclusion zone, Fig. 4) must be sufficient to initiate new crack growth.

This model of macrocrack growth predicts a number of precursory phenomena that will result from the physical processes that occur within the tertiary inclusion zone. These precursors will include the following: (1) The displacement rate above the primary inclusion zone will increase dramatically as cracks form within the tertiary inclusion zone. (2) Seismicity increase in the tertiary inclusion zone and electromagnetic phenomena in the epicentral region (assuming conditions favoring their existence are present), will become pronounced during the time duration of the class III precursor in response to the rapid increase in load and loading rate in the focal region of the primary inclusion [7, 49]. These increases will be in addition to those that developed during the class II precursor phase. (3) There will be a release of strain energy produced by macrocrack growth within the primary inclusion just prior to the initiation of catastrophic fault growth ('strong motion'). The time duration of this release is on the order of L_i/v_p, where L_i is the length of the primary inclu-

sion zone and v_p is the longitudinal wave velocity in the material just prior to the mainshock. Thus, the model predicts that there will be a release of 'low' frequency elastic energy prior to the initiation of strong motion (fault growth). The time duration of this energy release will be shown shortly to be a function of the magnitude (M) of the mainshock.

A detailed model of the dynamics of fault growth during the mainshock sequence and its role in aftershock formation has been discussed elsewhere [10].

Direct field observations of these predicted class III precursors are scanty, although there is some evidence of low frequency waves occurring before some strong earthquakes [41]. There is also evidence of low frequency waves recorded on long-period seismometers shortly before ($\sim$few seconds) the initiation of strong motion of some shallow earthquakes [S. T. HARDING, personal communication, 1975]. The phenomena of 'earthquake lights' and atmospheric electrical discharges have been documented to occur a few minutes or seconds prior to some strong earthquakes [49]. There is also some evidence of very short-term anomalous tilt prior to moderate earthquakes. For example, HARDING and KIRBY [personal communication, 1975], using long-period seismometers in the epicentral region of the August 1975 Yellowstone earthquake sequence, observed a tilt-like precursor approximately 0.2 sec prior to a number of aftershocks in the magnitude $M4$ range.

Lastly, there are three additional observations of the inclusion theory that deserve mention. (1) The direction of fault growth will be parallel to the direction of the local maximum principal stress at all times during the growth phase of the failure. Thus, while shear faulting would appear to violate the requirement that failure satisfy a minimum energy principle, that is, the fault forms at an angle to the applied stresses (σ_{10}, σ_{30}), this difficulty does not arise in the inclusion theory. The fault always grows parallel to the direction of the local maximum applied principal compressive stress (σ_1). (2) The Griffith theory is a limiting case of the inclusion theory since the equations reduce the Griffith equation when there is no elastic contrast between the inclusion and its surroundings [6]. However, the Griffith theory is strictly applicable only to describe the formation of the *first crack*, usually considered to form on the molecular level [23]. Once this crack(s) has formed, crack interaction effects must be considered to describe the further evolution of failure. (3) The inclusion theory predicts the existence of a critical confining stress when the behavior of the material changes from a brittle to a ductile deformation mode. This transition will occur when the ratio of the least principal far field stress, σ_{30}/σ_{10}, attains a value ($\sim 0.07 \rightarrow 0.10$) such that the tensile stress within the inclusion zone cannot attain the value σ_{t0}.

Precursor time–length relationship of failure

A diffusion-like functional relationship between precursor time and focal region area is predicted by the scale invariant properties of the inclusion theory [7]. Thus,

the relationship between the class I precursor time (τ_0) and the focal region area (A) of the primary inclusion zone of the impending failure can be written

$$\tau_0 = \alpha A, \tag{1a}$$

where α is a proportionality constant. Once the primary inclusion zone has formed, the process leading to the formation of the secondary cracks which will, in turn, coalesce with the primary cracks at the instant of the mainshock, begins. If A_c denotes the cross-sectional area of an average size crack within the primary inclusion zone, then the relationship between τ_0 and A_c can be written by virtue of the scale invariant properties of the inclusion theory

$$\tau_0 = \beta A_c, \tag{1b}$$

where β is a constant whose magnitude and relationship to α are determined below.

For simplicity, we shall assume that the average size crack which forms within the secondary inclusion zone just prior to failure can be modeled by a narrow penny-shaped geometry, that is, $A_c = (\pi/4)L_c^2$ where L_c denotes an average linear dimension of the secondary inclusion zone. Let us also assume that the scale invariant properties of the theory are applicable to some minimum average length, say $L_c = l_c$, that is on the order of a few molecular bond lengths. On this scale, l_c denotes the fundamental secondary inclusion length within which a crack of length l_c will form at the instant of failure. This crack may be nucleated at dislocations and/or other stress raisers, such as point defects (impurity atoms, vacancies). The energy required to form such a crack on this scale is of the order of a few electron volts (1 eV $= 1.6 \times 10^{-12}$ ergs) [23]. Thus, an order of magnitude estimate of l_c is 1×10^{-7} cm (see equation 10). Let v_p represent the longitudinal wave velocity in a physical system of this dimension. Major structural changes, in this instance, crack formation, cannot be predicted within this system in a time interval that is shorter than the characteristic time, l_c/v_p, of the system. Therefore, the relationship $l_c/v_p = (\pi/4)\beta l_c^2$ must be satisfied, or simply, the proportionality constant β is $(\pi/4)/l_c v_p$. Reasonable values of v_p and l_c on this length scale are 1×10^6 cm/sec and 1×10^{-7} cm, respectively. Hence, an order of magnitude estimate of the class I precursor time-crack area relationship is

$$\tau_0 \approx 10 A_c \quad (A_c \geq 10^{-14}\ \text{cm}^2), \tag{2a}$$

where τ_0 and A_c are measured in seconds and square centimeters, respectively.

Equation (2a) can be used to derive the functional relationship between τ_0 and what has been referred to in the literature as 'fault' length, L. 'Fault' length will be defined to be the average dimension of the aftershock region (focal region) whose area is denoted by A [2, 5, 11]. Let $L = \mu L_i$, where μ (≥ 1.0) is a scale invariant quantity relating the ratio of focal region length to primary inclusion length. Let γ denote the ratio of the average crack length (L_c) within the primary inclusion zone to the length of the primary inclusion zone (L_i). Equation (2a) can be written

$$\tau_0 \approx 10(\gamma/\mu)^2 L^2. \tag{2b}$$

A reasonable estimate of μ is 3.0, since the range of influence of an ellipsoidal-shaped inclusion is of the order of three times its length [22]. Experimental investigations by the Bureau of Mines of tilt and seismicity precursors in a wide variety of rock types indicate that in standard size laboratory specimens (5 cm in diameter, 10 cm in length), τ_0 and L are approximately $(1 \rightleftarrows 3) \times 10^{-3}$ sec and $1 \rightleftarrows 3$ cm, respectively [9]. Substituting these values into equation (2b) gives $\gamma = 1 \times 10^{-2}$, in good agreement with other independent measurements of crack size within the primary inclusion (see Fig. B1, Appendix B). Thus, an order of magnitude estimate of class I precursor time—focal region area relationship in rock materials is approximately $\tau_0 \approx 1.0 \times 10^{-4} A$, where τ_0 and A are measured in seconds and square centimeters, respectively.

It will be shown in the application section and Appendix C that rockbursts in northern Idaho, where the primary inclusion zone length, magnitudes, and class I precursor times are known, give an upper limiting value of the relationship between τ_0 and A. The result is

$$\tau_0 = 2.43 \times 10^{-4} A. \tag{3}$$

It is also shown that (for materials whose porosity is approximately zero) the ratio of focal region area to primary inclusion area is $A/A_i = 21.8$. According to the postulated scale invariant properties for failure, the evaluation of these parameters for a known failure is sufficient to describe the characteristics of all other failures.

Figure 5a illustrates the precursor time—'fault' length relationships that are observed for selected earthquakes, mine failures, and laboratory size rock failures [1, 9, 11, 34]. The fit of equation (3) to these data is shown for comparison. The relationship between precursor time and calculated average crack length ($L_c = (\gamma/\mu)L = 5.28 \times 10^{-3}L$) for these data is shown in Fig. 5b. Note that the predicted average crack lengths associated with the rock bursts are in the order of 10^2 cm. These length estimates also agree with independent calculations of crack lengths associated with the energy radiated by individual cracks in rockbursts ($\sim 10^{10}$ ergs). Note also that average crack lengths predicted to be associated with the dilatant zones of major crustal earthquakes, such as might occur at sites of major underthrusts and/or normal-faulting earthquakes along subduction zones, are of the order of a few tens of meters to a few hundred meters. These length predictions agree closely with crack lengths calculated elsewhere [8] that *induce* deep earthquakes by a void collapse mechanism.

The relationship between the time duration for the class II precursor time, τ_{s0}, focal region area (A), and average crack area (A_c) within the primary inclusion zone is readily determined from equations (2a) and (3). The result is

$$\tau_{s0} = 2.43 \times 10^{-4} A_c = 1.11 \times 10^{-9} A, \tag{4}$$

where τ_{s0} is measured in seconds and both A and A_c ($A_c = 10^{-4} A_i = 10^{-4} A/21.8$) are measured in square centimeters. It is assumed that no changes occur in the far-field stresses (strains) during τ_{s0}.

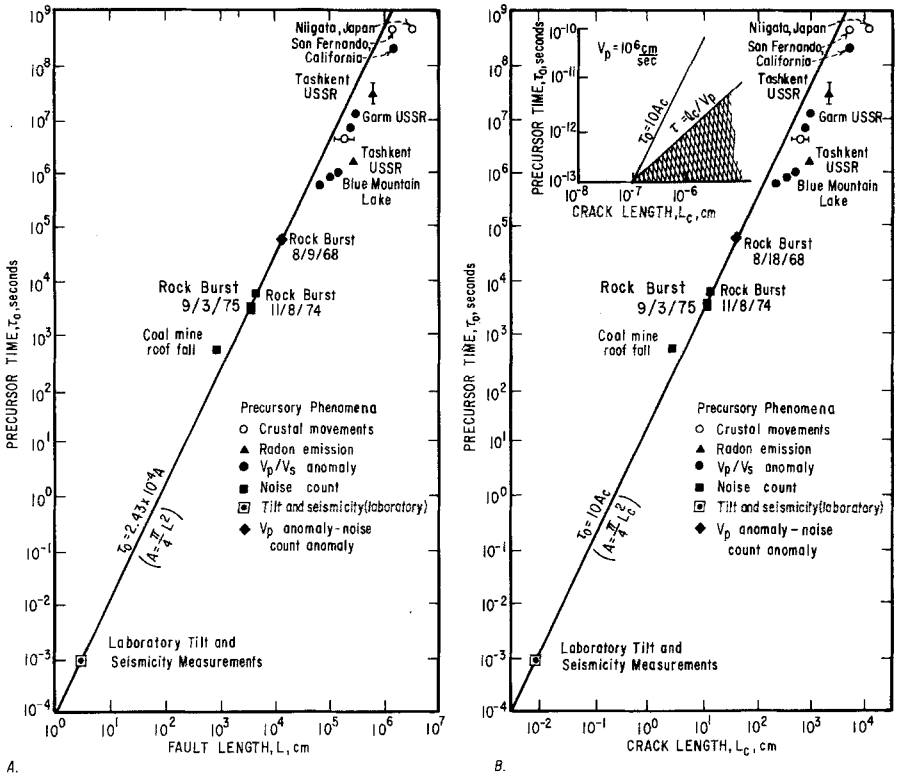

Figure 5
Precursor time–fault length (A)—Crack length (B) relationships of failure.

It is of value to express the class I and II precursor times in terms of the energy released as seismic radiation during the mainshock, or alternatively, the magnitude, M, of the mainshock. UTSU and SEKI [31] and MOGI [18] have observed that the aftershock area (A) of Japanese earthquakes can be related to magnitude by the relationship [recently revised by UTSU, 46, 53]

$$\log_{10} A = M + 6.3 \tag{5}$$

where A [$= (\pi/4)L^2$] is measured in square centimeters. Equations (3), (4), and (5) can be combined to give

$$\log_{10} \tau_0 = M + 2.68 \qquad \log_{10} \tau_{s0} = M - 2.65 \tag{6}$$

Table 1 lists predicted precursor times for class I and class II precursors for a range of magnitudes varying from $M(-)5$ to $M8$ failures. It is of interest to note S-bend tilt precursor times of nearly 0.6 hr, 6.2 hr, and 2.6 d are predicted to occur for mainshock magnitudes in the $M6$, $M7$, and $M8$ class, respectively. SASSA and NISHUMURA [28, 29] observed S-bend precursor time durations comparable to those predicted

Table 1

Predicted precursor times as a function of magnitude

(Note: no changes are assumed to occur in the far-field boundary conditions during the times τ_0 and τ_{s0})

Magnitude	τ_0	τ_{s0}	Comment
−5	4.8 m	0.02 μs	Typical laboratory size failure
2	13.3 hr	0.2 s	Typical mine failure
4	55.4 d	20.0 s	Earthquake
5	1.5 yr	6.5 m	Earthquake
6	15.2 yr	0.6 hr	Earthquake
7	152 yr	6.2 hr	Major earthquake
8	1520 yr	2.6 d	Great earthquake

by equation (6) prior to several major underthrust events in Japan. In addition, an S-bend tilt time of the order of 20 seconds is predicted to occur prior to a magnitude $M4$ earthquake. This value is large enough to suggest the use of S-bend tilt (and other class II precursors) as a possible indicator of impending moderately sized ($\geq M4$) earthquakes.

The relationship between the predicted class III precursor time, τ_{r0}, and an average dimension (L_i) of the primary inclusion zone is

$$\tau_{r0} = \frac{L_i}{v_p}, \tag{7}$$

where v_p is the longitudinal wave velocity in the focal volume just prior to the mainshock. The relationship between τ_{r0} and magnitude is found from equations (5) and (7a)

$$\log_{10} \tau_{r0} = 0.5M + 2.8 - \log_{10} v_p \tag{7b}$$

Thus, for a typical longitudinal velocity of 3×10^5 cm/sec, the predicted class III precursor times for earthquakes magnitudes of $M4$, $M5$, $M6$, and $M7$ are 0.2 s, 0.6 s, 2 s, and 6.2 s, respectively. These times represent the minimum time interval between the initiation of macrocrack growth and the initiation of fault motion at the fault-macrocrack zone. Note also that the predicted polarities of these motions will be opposite to one another.

HARDING and KIRBY (1975, personal communication) observed low frequency 'tilt' precursors, recorded on long period seismometers, whose time durations were of the order of 0.2 s prior to aftershocks in the $M4$ range in the August 1975 Yellowstone mainshock ($M6.2$). The observed polarities of these precursory events were opposite to the seismic event they preceded. SPENCE (personal communication, 1976) has also observed precursory events occurring at intervals of the order of 1 s prior to subterrace normal faulting events following the 1965 Rat Island mainshock. The body wave magnitudes of these events were in the range of 5.2 to 5.6. The precursory events were also of opposite polarity to the event they preceded.

Relationship of the class I precursor time to mainshock magnitude

In the inclusion theory of failure, a macrocrack zone that contains an open void of cross-sectional area A_i forms within the primary inclusion zone prior to the mainshock. The total change in the elastic potential energy, Ψ, of the system provides the energy required for the failure. When the boundaries far removed from the primary inclusion zone are rigidly fixed, no work can be done by the far-field stresses (σ_{10}, σ_{20}, σ_{30}). Thus, the change in the elastic potential energy is equal to the decrease in the strain energy of the system. If, on the other hand, the far-field stresses are constant during the mainshock, work will be done by these stresses and the strain energy of the system will decrease. However, the change in the elastic potential energy of the system is the same as in the case where the boundaries are rigid. Consequently, the total potential energy change, Ψ, is the difference between the total strain energy for the medium with and without the void. The result of this calculation is [4, 27, 26, 32]

$$\Psi = \frac{(1 - \nu_0^2)}{\pi E_0} \sigma_0^2 L_i^3, \tag{8}$$

where ν_0 and E_0 are the intrinsic values of Poisson's ratio and Young's modulus of the medium, σ_0 ($\sigma_0^2 = \sigma_c^2 \sin^2 \beta + \sigma_t^2 \cos^2 \beta$) denotes the 'effective' stress existing within the primary inclusion zone, and β is the angle between the major axis of the macrocrack and the axis of the maximum principal compressive stress (σ_c). As this angle is zero (Fig. 2), the 'effective' stress is $\sigma_0 = \sigma_t$.

Equations (3) and (10) can be combined to give

$$\Psi = 1.19 \times 10^3 \frac{1 - \nu_0^2}{E_0} \sigma_t^2 \tau_0^{3/2}, \tag{9}$$

where $L_i = L/4.67$. The relationship between Ψ and the magnitude of the mainshock is found by combining equation (6) and (9). The result is

$$\log_{10} \Psi = 7.10 + \log_{10} \frac{1 - \nu_0^2}{E_0} \sigma_t^2 + 1.50M, \tag{10}$$

where Ψ is measured in ergs. The appropriate value of σ_t to be used in equation (10) must be the theoretical tensile strength of the material because this is the stress required to form a void of length L_i. This strength is estimated to lie between the limits $\frac{1}{30}E_0 \leq \sigma_t \leq \frac{1}{10}E_0$ [23]. We shall use an average value of $\sigma_t = \frac{1}{20}E_0$ in the following calculations. Appropriate values of E_0 and ν_0 for brittle materials are 1×10^{12} dynes/cm^2 and 0.30, respectively. Thus, the average change in the total potential energy of a system within which a void of length L_i forms prior to failure is approximately

$$\log_{10} \Psi = 16.5 + 1.5M. \tag{11}$$

The energy provided by the decrease in the potential energy, Ψ, will be partitioned during the failure in the form of heat generated by friction along the fault(s), crack closure, plastic deformation, and seismic wave radiation. Thus, the total change in potential energy of the system can be written

$$\Psi = \Psi_p + \Delta\Psi, \tag{12}$$

where Ψ_p $(=\Psi_r + \Psi_d)$ represents the energies radiated by seismic waves and dissipated by inelastic processes as the fault(s) and its associated inclusion(s) advances into the focal region of the primary inclusion and $\Delta\Psi$ denotes the reversible component of Ψ required to complete the failure preparation process. Ψ_p denotes the energy required to form the primary inclusion zone of the impending failure. *This energy must be supplied by the seismic events that form the primary inclusion zone.*

The energy radiated by the mainshock will be assumed to be given approximately by the Gutenberg–Richter relationship

$$\log_{10} \Psi_r = 11.8 + 1.5M. \tag{13}$$

This relationship should be considered to represent only the average energy that can be radiated by an earthquake since the radiated energy will obviously be dependent on both the material properties and the stress conditions persisting in the hypocentral region of the mainshock.

The energy, Ψ_d, required in the formation of the primary inclusion zone of the mainshock represents a maximum value of the energy available for aftershocks, assuming of course, that the system approaches an equilibrium state following the mainshock. To determine the functional relationship of Ψ_d to Ψ_p, we shall require an understanding of the processes required to form the primary inclusion. First, recall that one of the more distinguishing characteristics of the primary inclusion zone of an impending failure is the existence within this zone of a tensile stress that is oriented normal to the direction of eventual rupture propagation. This direction is parallel to the direction of the local maximum principal stress axis (σ_1, Fig. 2b) within the deformation band that is itself contained within the anomalous or dilated volume. Thus, shear failure, as defined in this article, *cannot* occur within the primary inclusion zone. Consequently, seismic events that produce the primary inclusion zone *will not be followed by aftershocks*, or at the very least, will exhibit a severely curtailed aftershock sequence. These events will be characterized by anomalously long rupture lengths. The regions fractured by these seismic events form the volume of the primary inclusion zone of the forthcoming mainshock. Of course, the energy, Ψ_d $(=\Psi_p - \Psi_r)$ that would normally have been available for frictional dissipation and aftershocks for each of these events becomes available to fracture a region much larger than the individual focal regions of the individual events.

Equations (11) and (13) can be combined to give the equivalent magnitude of each seismic event that forms the primary inclusion zone. The result is

$$M^* = M_n + 3.1 \tag{14}$$

where M_n represents the magnitude of the event had it not been involved in forming the primary inclusion zone. Since $\Delta\Psi^* = \Psi^* - \Psi_p^* \approx \Psi^*$, it can be assumed that *all* the energy that would have normally been dissipated by frictional sliding and aftershocks is available to fracture a portion of the evolving primary inclusion zone. Thus, M^* in equation (14) represents an upper limiting value to the equivalent magnitude. The effective area, A^*, fractured by these events is found by equation (5) to be

$$A^* = 10^{3.1} A_n \tag{15}$$

Let A_i denote the area of the primary inclusion zone of the forthcoming mainshock. If n denotes the number of seismic events, of average equivalent magnitude M^*, then $nA^* = A_i$, where the areas of the individual primary inclusion zones that give rise to each of the n events are neglected. The scale invariant properties of failure and experimental data (see Appendix B) give an order of magnitude estimate of the ratio of A_i and A_n, A_i/A_n, to be 1×10^4. Thus, an upper limit to the required number of events, of equivalent magnitude M^*, predicted to form the primary inclusion zone is

$$n \approx 1 \times 10^4 \frac{A_n}{A^*} \approx 10. \tag{16}$$

This value is shown to be close to values observed prior to moderate rock bursts and moderate earthquakes in the application section. Equations (15) and (16) can be combined to give

$$\begin{aligned} \log_{10} n &= \log_{10} A_i - \log A^* \\ &= \log_{10} A - \log A_n - 4.3 \end{aligned} \tag{17}$$

where A ($= 21.8A_i$) represents the focal region area of the primary inclusion zone. Equation (17) provides an estimate of the upper limiting value of the difference in magnitude between the impending mainshock, M, and the average magnitude, M_n, of the 'background' seismic events that occur prior to the formation of the deformation band within which the primary inclusion zone,

$$\Delta M = M - M_n = 5.3. \tag{18}$$

In addition, note that equation (18) can be interpreted as indicating that if $M_{\max}$ denotes the maximum value of the average 'background' seismicity, then an *upper limiting value* of the magnitude of an earthquake that this region can sustain is $M_{\max} + 5.3$.

The energy, Ψ_p, required to form the primary inclusion zone is simply

$$\begin{aligned} \log_{10} \Psi_p &= \log n + 16.5 + 1.5M^* \\ \log_{10} \Psi_p &= 14.2 + 1.5M, \end{aligned} \tag{19}$$

where for calculational purposes it is assumed that each of the n events that form the primary inclusion zone is equivalent. Thus, the energy partitioning of failure predicted by the inclusion theory is approximately

$$\begin{aligned} \Psi_r &= 0.004\Psi_p \\ \Psi_d &= 0.996\Psi_p \\ \Psi_p &= 0.005\Psi \end{aligned} \tag{20}$$

Equation (20) shows that the seismic efficiency factor, η ($\eta = \Psi_r/\Psi_p$), for failures satisfying the constraints of the inclusion theory and the Gutenburg–Richter relationship is only 0.40%. Similarly, of the total energy available for aftershocks, only 0.40% will be available for seismic radiation. Thus, the model predicts that, at the very minimum, approximately 0.5% of the total energy radiated by the mainshock will be radiated by all of its aftershocks. In addition, the functional relationship between the total energy radiated by the aftershock sequence, $\Psi_r^{(as)}$, and Ψ_r can be written

$$\log_{10} \frac{\Psi_r^{(as)}}{\Psi_r} = 1.5\, \delta M, \tag{21}$$

where $\delta M = M - \overline{M}$ and $\overline{M}$ denotes an upper limiting magnitude to the largest possible aftershock. Equations (20) and (21) give this value of $\overline{M}$ to be $M - 1.6$, or simply, the predicted maximum value of the magnitude of any aftershock within the aftershock sequence is the magnitude of the mainshock less 1.6. This result is close enough to and thus lends theoretical support to the well-known empirical relationship referred to as Bath's law, that the largest magnitude of an aftershock within an aftershock sequence is $M - 1.2$ [50].

The above analysis suggests a method of determining the average linear dimensions, l_0, of the anomalous zone within which a shock of magnitude M can occur. The modified Utsu relationship can be written for the mainshock as

$$\begin{aligned} \log_{10} A &= M - 3.7 \\ &= M_n + 1.6, \end{aligned} \tag{22}$$

where M_n denotes the 'average background' seismicity and A is the minimum area in km^2 that can support this level of seismicity. Thus

$$A = 39.8 \times 10^{M_n}, \tag{23}$$

and if l_0 denotes an average linear dimension of the anomalous region, equation (23) leads to the relationship

$$l_0 \leq 8.9\sqrt{(2/\pi)} \times 10^{0.5 M_{\max}}, \tag{24}$$

Equation (24) should be considered as specifying the *minimum average* linear dimension of an assumed circularly-shaped anomalous region that can sustain an average 'background' seismicity of maximum value $M_{\max}$. By way of example of equation

Table 2

Typical minimum dimensions of anomalous region and earthquake magnitude

($M = M_{max} + 5.3$; $\log_{10} A = M_{max} - 3.7$; $A_i = A/21.8$)

M_{max}	M	A, km^2	A_i, km^2	l_0 km	Remarks
−5	0	2×10^{-9}	9×10^{-11}	2×10^{-2}	Typical laboratory size failure
−2	3.3	2×10^{-6}	9×10^{-8}	0.80	Typical mine failure
1	6.3	2×10^{-3}	9×10^{-5}	25.0	Earthquake
2	7	2×10^{-2}	9×10^{-4}	80	Earthquake
3	8.3	0.20	9×10^{-3}	250	Earthquake
3.3	8.6	0.64	3.0×10^{-2}	450	Earthquake

(24), Table 2 lists several typical values of l_0 against M_{max} as well as the value *maximum* allowable magnitude, M, of an earthquake that can occur within this region.

Geodetic investigations in seismically active regions indicate that the spatial extent of the anomalous region is often much larger than the focal volume of the earthquake itself. For example, premonitory changes were detected as far as 100 km from the epicenter of the 1964 Niigata earthquake ($M7.5$) [38] and nearly 25 km prior to magnitude 3 events in the Garm region [39]. AGGARWAL *et al.* [2] observed the size of an anomalous zone to be at least 10 km prior to a magnitude 3.6 event in the Blue Mountain Lake region of New York state. Equation (24) shows that the calculated minimum dimension (l_0) for the Niigata mainshock must be at least 90 km ($M7.5$). The calculated range of l_0 is approximately 20 km to 200 km for 'background seismic events' in the magnitude range of $M_{max} = 1.0$ to 3.0 in the Garm region. The calculated size of the anomalous region at Blue Mountain Lake is in the range of 10 km. The typical magnitude of the 'background' seismicity is in the order of 1.0 in this region [2].

Factors affecting the precursor time focal region area-magnitude relationships of failure

The functional relationship between the class I precursor time (τ_0) and focal region area (A), where $A = (\pi/4)L^2$, can be written

$$v_0 = \frac{L}{\tau_0} = 5.24 \times \frac{10^3}{L} \text{ cm/sec}, \tag{25}$$

where v_0 denotes the average velocity of the crack closure front in the focal region of the primary inclusion zone when the far-field stresses (strains) remain constant during the time duration of the class I precursor. Equations (5) and (25) show that this velocity is magnitude dependent, that is, the larger the magnitude, the smaller the closure front velocity. For example, typical values of L on the laboratory scale [$M(-)5$] and major shallow earthquakes ($M8$) are calculated from equation (5) to

be in the order of 1 cm and 10^7 cm, respectively. These length values suggest closure front velocities in the order of 10^3 cm/sec and 10^{-3} cm/sec, respectively. Note that an upper limiting value of v_0 must be v_p.

When a condition arises such that changes (increases) in the far-field stresses (strains) can occur at a velocity v, where $v \geq v_0$, then the crack closure front *will proceed* at the higher velocity v in the focal region. In this instance, the *correct* class I precursor time, τ, is $\tau = L/v$. The precursor time-focal region area relationship becomes

$$\tau = \tau_0 \frac{v_0}{v} = 2.43 \times 10^{-4} \left(\frac{v_0}{v}\right) A. \quad (v \geq v_0) \tag{26}$$

As an example of equation (26), consider a magnitude $M7.5$ earthquake. Equations (3), (5), and (25) give τ_0, A, and v_0 to be approximately 244 yr, 3.16×10^3 km^2, and 0.26 km/yr, respectively, for this event. However, when changes in the far-field stress (or strains) are occurring at a velocity, say of the order of 50 km/yr, as is *observed* and *predicted* to occur in major shallow earthquake zones [8, 18], then the predicted *actual* class I precursor time for this hypothetical event becomes $\tau = \tau_0$ (0.26/50) = 1.27 yr, *a reduction in what would have been the predicted time by nearly two orders of magnitude*. This example serves to illustrate that the class I precursor time–area relationship, as specified by equation (3), must be used with extreme caution. However, this relationship can be modified to take into account changes in the far-field boundary conditions once it has been determined how the boundary conditions are changing.

Observational data for large earthquakes ($\geq M6$) suggest that there is little or no correlation between earthquake magnitude and what has been referred to as the class II precursor time (τ_{s0}) in this article [46]. Yet equation (6) suggests that τ_{s0} and M are functionally related to one another. It is of interest, therefore, to consider whether changes in the far-field boundary conditions, such as might occur owing to tidal strains, can influence or possibly trigger earthquakes. Earthquakes that would be triggered by such short-term changes in the far-field boundary conditions would give the appearance of exhibiting little or no positive correlation between τ_{s0} and magnitude. This will be particularly true for those large earthquakes where the phase of secondary crack growth within the primary inclusion begins or is occurring during the time interval when tidal effects are increasing the value of σ_t within the primary inclusion zone.

The lunar tidal stress is known to have a peak amplitude of approximately 5×10^4 dynes/cm^2, cycled every 13 h, in the crust. The peak rate of change of the tidal stress is about 7 dynes/cm^2/sec [49]. Let us assume that the average Young's modulus of the primary inclusion zone is in the order of 1×10^{11} dynes/cm^2. Thus, the peak volumetric strain, ε, that can be induced within the primary inclusion zone is in the order of $\varepsilon \simeq 5 \times 10^{-7}$. *The problem of resolving whether the lunar tidal stress can trigger an earthquake rests with a determination of whether this stress can initiate*

or accelerate the formation of cracks that will eventually lead to the formation of the secondary cracks that, in turn, will coalesce with the primary cracks (Fig. 2d) and thus produce the earthquake.

Theoretical and experimental results discussed earlier in this article have shown that an order of magnitude estimate of the area, A_c, of the secondary cracks is $A_c \simeq 1 \times 10^{-4} A_i$, where A_i is the area of the primary inclusion. Since the cracks that produce the secondary cracks form in a tensile stress field, the area of these cracks is approximately $a_c \simeq 1 \times 10^{-3} A_c \simeq 1 \times 10^{-7} A_i$ by equation (15). The relation of a_c to the area, a_{ci}, of the primary inclusion zone that produces this crack is $a_{ci} \simeq 1 \times 10^{-7} A_i / 21.8 \simeq 4.6 \times 10^{-9} A_i$. If l_{ci} denotes the length of this inclusion zone, then $l_{ci} \simeq 6.8 \times 10^{-5} L_i$. It is shown in Appendix D that an order of magnitude estimate of the thickness, t_{ci}, of these cracks is αl_{ci}, where α, of the order of 1×10^{-3}, is their aspect ratio. Consequently, an order of magnitude estimate of the volumetric strain, ε^*, that will be induced within the primary inclusion zone as a result of crack growth within the secondary inclusion zone is $\varepsilon^* = t_c^*/L_i \sim 6.8 \times 10^{-8}$. This value compares with the peak strain of $\varepsilon \sim 5 \times 10^{-7}$ that can be induced within the primary inclusion zone by tidal strains, and is suggestive that induced tidal strains are of sufficient magnitude to initiate crack growth within the primary inclusion zone *once this zone has approached a critical state.* In addition, these calculations show that the tidal strains can induce strains within the secondary inclusion zones that are several orders of magnitude greater than the strains required to induce the level of crack growth that will, in turn, lead to the development of those cracks that form the secondary inclusion zone. Therefore, those earthquakes whose size is sufficiently large that their secondary inclusion zones begin to form during the time interval that the tidal stresses are increasing may be triggered by this stress increase. Such earthquakes, particularly those of large magnitude, may give the misleading appearance of exhibiting class II precursory phenomena whose time durations (τ_{s0}) appear to be independent of magnitude. Thus, the apparent lack of a significant correlation between τ_{s0} and M [46] may be explained by changes induced within the far-field boundary conditions resulting from the influence of lunar tides. This hypothesis could be treated by monitoring class II precursors of small shocks whose magnitude is small, say $\leq M4$, and determining the relationship of τ_{s0} to M for these events. Detailed monitoring of rockbursts may be useful in this respect.

The effect of changes in the applied far-field stresses (σ_{10}, σ_{30}) will produce *no* change in the amount of energy released by the failure. However, the same cannot be said when fluids under a pressure, P_f, are present in the focal volume. For example, when fluids are present within the anomalous volume, the principal stresses (σ_1, σ_3) within this volume will each be reduced by an amount approximately equal to P_f. Consequently, less strain energy can be stored within the anomalous volume and subsequently released during the mainshock. Thus, the predicted magnitude, say M_p, of a failure occurring within a volume containing fluids under pressure will be greater than the observed magnitude M.

Equation (9) can be readily applied to this situation to give the total potential energies for the 'dry' (Ψ_0) and 'wet' (Ψ) cases

$$\log_{10} \Psi_0 = 3.08 + \log_{10} \frac{1 - \nu_0^2}{E_0} \sigma_0^2 + 1.50 \log_{10} \tau_0 \quad \text{'Dry'}$$
$$\log_{10} \Psi = 3.08 + \log_{10} \frac{1 - \nu_0^2}{E_0} \sigma_{\text{eff}}^2 + 1.50 \log_{10} \tau_0, \quad \text{'Wet'} \tag{27}$$

where $\sigma_{\text{eff}}/\sigma_0 = (\sigma_3 - P_f)/\sigma_3$, σ_3 is the least principal stress existing within the anomalous zone, and *no* changes are assumed to occur in the far-field tectonic stresses (strains) during the time duration of the class I precursor. Equations (10) and (27) can be combined to give the discrepancy between the predicted and observed magnitudes to be

$$M = M_p + \tfrac{4}{3} \log_{10} \frac{\sigma_{\text{eff}}}{\sigma_0} \quad (M \leq M_p) \tag{28}$$

As an example, *assume the difference between the predicted and observed magnitudes* is 1.0. Equation (28) predicts that the magnitude discrepancy can be readily explained by the presence of a pore fluid in the focal volume of the mainshock with a pressure P_f equal to approximately 80% of the *local* far-field *minimum* principal stress. Local, in the context used here, refers to the stresses existing within the anomalous volume in which the failure occurs.

Two important practical results arise from equation (28). (1) The existence of pore fluids in an earthquake zone will produce a discrepancy between the predicted (M_p) and observed magnitudes (M) of the earthquake ($M \leq M_p$). There will be *no* discrepancy in the predicted precursor time τ_0 provided the far-field tectonic stresses remain constant during the precursor time duration τ_0. (2) The decrease in observed magnitude M as P_f is increased will be evidenced by a transition from unstable to stable formation. This predicted behavior has been observed experimentally by MARTIN [1975, personal communication]. *This result suggests that earthquake prone regions exhibiting swarm activity may be characterized by high values of* P_f/σ_3.

Application to existing earthquake regions

The application of the seismic conditions discussed above that are required to predict earthquakes is made in this section. The seismic conditions include the magnitude, seismicity, and the spatial and temporal distribution of seismicity in and near the pending rupture zone. Five earthquake sequences are investigated and have been chosen so as to illustrate the predictive capability of the inclusion theory and, in particular, to point out some of the difficulties that can and will occur in the development of any reliable predictive capability for earthquakes. These examples

include: (1) The 3 September 1975, Rockburst, Star mine, Burke, Idaho; (2) The Garm Earthquake of 22 March 1969; (3) The 9 February 1971, San Fernando, California, Earthquake; (4) The August 1973, Earthquake at Blue Mountain Lake, New York; (5) The 3 October and 9 November 1974, Peru Earthquake sequence.

The 3 September 1975, rockburst, Burke, Idaho

A moderate rockburst occurred on the 7500 level of the Star mine, Burke, Idaho, at 10:09 a.m. (18:09 UTC) on 3 September 1975. The burst was preceded by a dramatic increase of seismic activity that was followed by a distinct decrease prior to the burst. Miners were evacuated from an active mine stope located in the immediate vicinity of the eventual burst hypocenter. Detailed information of the Star mine and the mining method used in this mine are available elsewhere [12]. Location accuracy of the seismic events in this mine is ± 4 m.

Table 3
Seismic event number and time prior to burst

Event number	Time (a.m.)	Event number	Time (a.m.)	Event number	Time (a.m.)
1*	9:00:32	11	9:02:32	21	9:30:40
2	9:00:38	12*	9:02:40	22	9:44:52
3*	9:00:48	13*	9:03:00	23	10:01:03
4*	9:00:53	14*	9:03:38	24	10:01:58
5	9:00:55	15	9:05:53	25	10:02:08
6*	9:00:57	16	9:06:09	26	10:02:24
7	9:01:11	17	9:06:46	27	10:02:42
8*	9:01:38	18	9:10:44	28	10:05:10
9*	9:01:39	19	9:22:27		
10	9:02:29	20	9:24:32		

Burst was event number 29 and occurred at 10:09:04 a.m.
* Refer to seismic events that formed the primary inclusion zone.

Table 3 lists the seismic event numbers and their corresponding times of occurrence prior to the burst. Figure 6a shows the event location numbers as well as the seismic events, termed aftershocks, that followed the burst. Figure 6(a,b,c) illustrate the seismic events as projected onto the horizontal plane (a), the projection of the aftershocks onto the vertical plane along sections A–A′ (b) and B–B′ (c). There are a number of results that are noteworthy from this data. First, the rapid increase of seismic activity prior to the burst was essentially associated with events 1 through 14 (Table 3). The seismicity increase was associated with the formation of the circularly shaped zone (shaded region, Fig. 6a) whose area, A_i, is approximately 7.86×10^5 cm^2. The total time required to form this zone was 188 s. Second, the seismic events that followed the formation of this zone were concentrated outside this zone, and were primarily located near and outside the boundaries of what was to be the aftershock

region. There was a slight increase in seismicity in the hypocentral region (events 24 and 25) approximately ten minutes prior to the burst. Third, the burst occurred at 10:05:10 a.m. (18:05:10, UTC) and was followed by 22 aftershocks that defined an elliptically shaped zone of approximately area, A, equal to 1.74×10^7 cm^2. The total time to the burst, measured from the initiation of growth (9:00:32 a.m.) of the primary inclusion zone, was 68.5 m. Fourth, the cross-sections of the aftershock zone reveal an elliptically shaped zone (Fig. 6b) whose major axis is parallel to the inferred rupture propagation direction as well as a circularly-shaped zone (Fig. 6c) normal to this direction. The observed geometry is remarkably similar to the aftershock zone geometry that is predicted by the inclusion theory when the local least and intermediate principal stresses are equal. This observation is also consistent with stress measurements on the 7300 level by S. CHAN [personal communication, 1976]. Chan's measurements show that the intermediate (σ_2) and least (σ_3) principal stresses are equal (Table 4). The major horizontal stress (σ_1) is probably of tectonic origin. Fifth, the inferred rupture propagation direction, that is, the direction where most of the energy was released (section A–A', Fig. 6a), was approximately normal to the vein

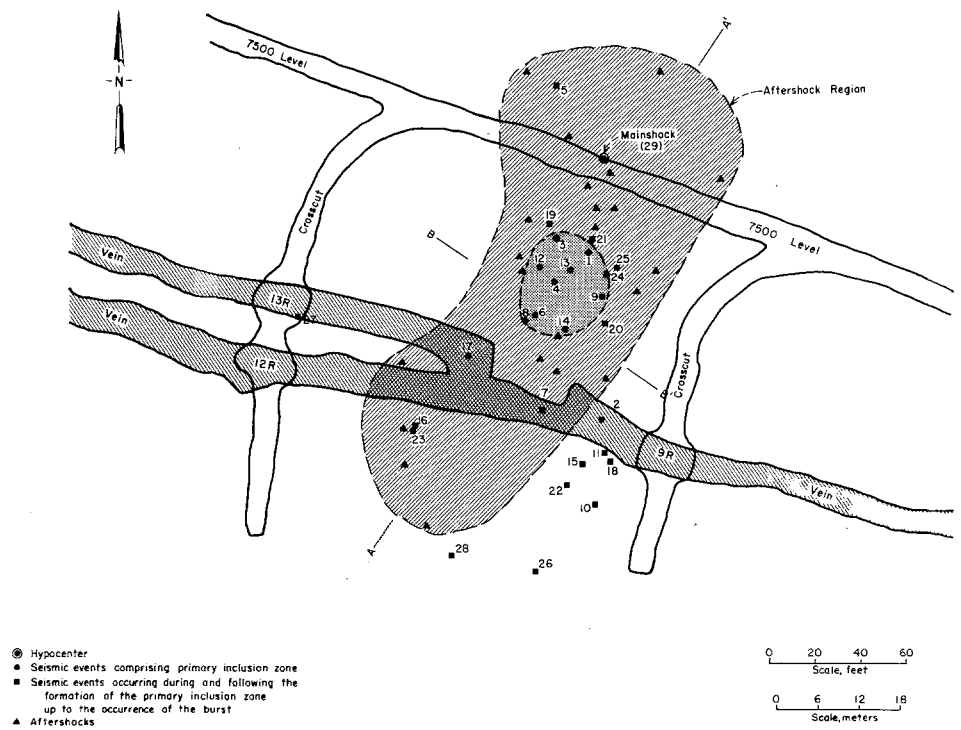

Figure 6a

Plan view of the 7500 level of the Star Mine, Burke, Idaho. A. Plan view of aftershock region, primary inclusion zone and burst hypocenter. B–C. Vertical sections of aftershock region along sections A–A' (B) and B–B' (C). D. Seismic count versus time in 4 September 1975 rockburst.

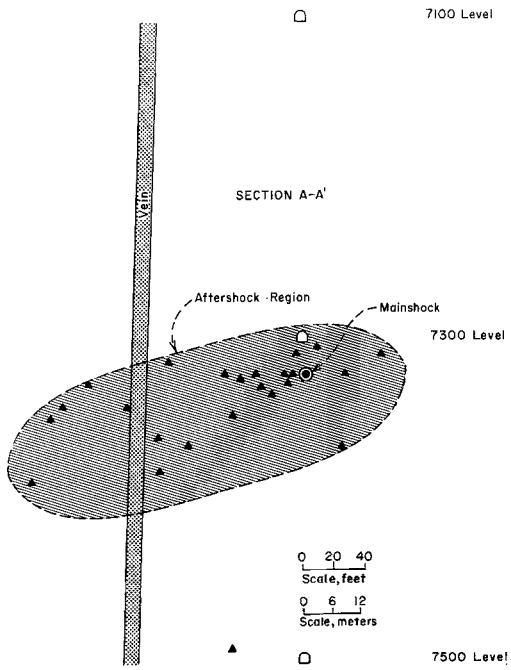

Figure 6b

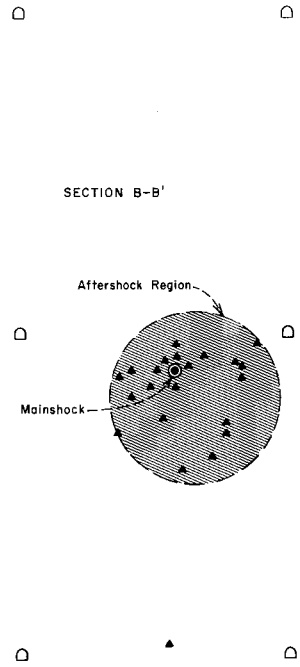

Figure 6c

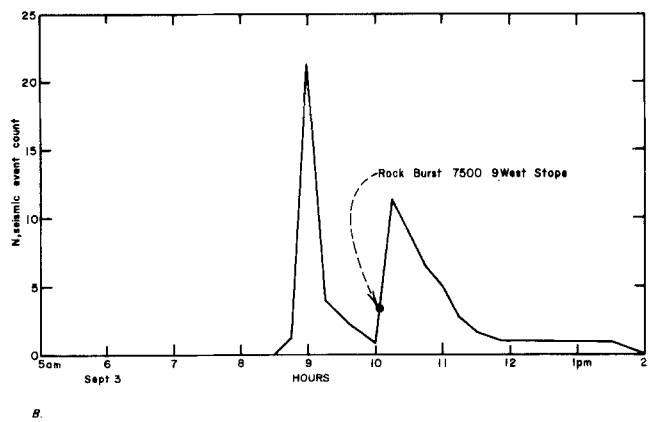

Figure 6d

Table 4
In-situ stress distribution at east lateral drift 7300 level—star mine
(CHAN, personal communication, 1976)

Stress	Magnitude	Bearing
Major horizontal (σ_1)	0.66 kb	N 14° W
Major horizontal (σ_3)	0.42 kb	N 76° E
Vertical (σ_2)	0.43 kb	—

(1 kb = 1 × 10^3 b, 1 b = 15 psi)

and, in particular, normal to the region where active mining was in progress. Major structural damage to the mine workings was observed in this area following the occurrence of the burst. Sixth, the burst hypocenter in Fig. 6 appears to be displaced approximately 6 m from the edge of the circularly-shaped zone, termed the primary inclusion zone. However, the burst is located using velocity surveys taken prior to the burst. Thus, as the focal volume of the primary inclusion zone begins to store strain energy, the seismic velocities in this volume will increase, thus giving rise to an apparent displacement of the burst hypocenter from the theoretically predicted location on the boundary of the primary inclusion zone.

Independent studies (reported in Appendix C) by the Bureau in the Galena mine, Wallace, Idaho, have shown that a lower limit to the ratio τ_0/τ_{d0} is 12.5. Consequently, once τ_d is known, a *minimum* predicted time to the burst is possible. The calculated time to the 3 September burst is 40 m, where the observed value of 188 sec is used for τ_d. This value compares favorably with the observed value of 68.5 m. However, based upon the observed areas A_i and A_0, the calculated times τ_{d0} and τ_0 are 191 sec and 70.3 m, respectively, in good agreement with the observed times of 188 sec and 68.5 m. Thus, not only was this burst predicted, the analysis admits a more realistic estimate of the ratio τ/τ_d (=21.8) required for future accurate prediction times. This analysis provides the physical basis for using this ratio in this article.

Lastly, this rockburst was not detected by the Newport, Washington, seismic station. The Newport station is capable of detection of events of magnitude $M1.5$ in the Coeur d'Alene district [KERRY, personal communication, 1976]. The functional relationship between aftershock area, A, and magnitude, M, is $\log_{10} A = M + 6.3$, where A is measured in square centimeters. Substituting the observed area of 1.74×10^4 cm^2 into this relationship gives a calculated magnitude for the 3 September burst of $M0.9$. This value is well below the threshold value of $M1.5$.

The 22 March 1969, M5.7 Garm earthquake

This earthquake was located 25 km from the Garm seismic station at a depth of 15 km [19]. All precursor observations were obtained within a radius of 25 km of

the epicenter and outside the 6 km by 10 km aftershock zone. NERSESOV *et al.* [19] have suggested that the precursor volume exceeded the source dimensions by a factor of five for this seismic event.

NERSESOV *et al.* and WYSS [19, 35] have summarized five independent precursor observations of this earthquake. (1) The seismicity decreased outside the epicentral region 1.7 to 1.5 yr prior to the mainshock. (2) The compression axes, obtained from fault plane solutions of small earthquakes located within the precursor volume, showed evidence of rotation approximately 1.7 yr before the mainshock; this reorientation of the compression axis was then followed by another rotation of 90°, approximately 3 months before the event. (3) The P-residual increased 0.4 sec at 1.2 yr prior to the mainshock [35]. (4) The resistivity began to decrease about simultaneously with the return to normal of v_p approximately 6 months before the earthquake. This change was measured at 10 km to the north of the epicenter. The calculated source radius for this shock was approximately 3 km. (5) The rate of uplift near the Garm station began to increase 1.7 yr prior to the mainshock.

The calculated magnitude for an event producing an aftershock area of 60 km^2, assuming the Utsu relationship (equation (5)) is applicable to this region, is found from equation (5) to be $M_p5.5$ as compared with the observed value of $M5.7$. The calculated minimum diameter (l_0) of the anomalous region, within which the mainshock occurred, is approximately 125 km. This calculation is based on observational data suggesting that this region sustains an average *maximum background* seismicity of magnitude $M_{\max} = 2.5$ [19]. Thus, the calculated ratio of l_0/L for this seismic event ($M_p5.5$) is approximately 12.5 for a source dimension, L, of 10 km. This value compares with the observed value of 5.0 [19].

In the *absence* of changes in the far-field stresses (strains) during the preparation time required for this event, the calculated precursor time, τ_0, for a mainshock of calculated magnitude $M_p5.5$ is 4.8 yr. The observed precursor time, τ, for this earthquake is estimated to be 1.7 yr [19, 35]. Because most major earthquakes occur in active tectonic zones, such as the Garm region, it is doubtful that the tectonic boundary conditions would remain constant during the predicted precursor time τ_0, and the corrected precursor time is now given by equation (26). However, once it is determined how these changes affect the predicted precursor time, the theoretical relationship between τ_0 and A (or M_p) can be appropriately modified and used to provide more accurate long-range prediction of future seismic events of comparable magnitude that might occur in this region. For example, equation (26) shows that the ratio between the velocity (v_0) of the crack closure front when the boundary conditions are changing is $v_0/v = \tau/\tau_0 = 0.35$ ($v_0 = 10$ km/4.8 yr $= 2.08$ km/yr) for the Garm region. Thus, for earthquakes of comparable magnitude in this region, the calculated precursor time–focal area relationship is $\tau = 8.60 \times 10^{-5} A$, where τ and A are measured in seconds and square centimeters.

The calculated time, τ_{d0}, required to form the primary inclusion zone of the 22 March 1969 mainshock is found from equation (C.5) and the experimentally

determined ratio of A_i and A ($A_i/A = 1/21.8$). The result is 4.3 months. The predicted times required to form the individual seismic events, whose predicted magnitudes, M_p, are determined from equation (18) to be approximately 0.4 are only 0.3 hr. Since this time interval is short enough that changes in the far-field stresses are negligible, the predicted time of 4.3 months is probably a reasonable estimate for the formation of the primary inclusion zone. It is important to note that this time interval will represent the time required for the seismic compression axes to change over to their new orientation. This calculated time is in reasonable agreement with the observed time ($\sim$6 months, see Fig. 2, reference 35).

It is noted that in the context of the inclusion theory, the focal region of an impending failure must become elastically stiffer than the surrounding anomalous volume during the latter portions of the earthquake preparation process. Thus, the stress difference will increase both within the focal region and throughout the anomalous volume in the plane of the primary inclusion and focal region zones. If the increase in stress difference is sufficient to initiate seismic events, then their compression axes will be rotated 90° to those associated with the seismic events that were produced by crack closure. The compression axis of the mainshock will be identical in orientation to the axes of those events that occurred in the pre-primary inclusion phase. This predicted behavior is in agreement with Soviet observations [19].

The San Fernando, California, earthquake of 9 February 1971

WHITCOMB *et al.* [34] have proposed that the dilatancy–diffusion model may be applicable to the San Fernando, California, earthquake (M6.4) of 9 February 1971. According to their interpretation, a large precursory change in the seismic body-wave velocities occurred approximately 3.5 yr prior to the mainshock. It is of interest to examine this earthquake from an alternative point of view.

Figure 7a illustrates the major tectonic features in the region surrounding the mainshock and its associated aftershock area [51]. The aftershock area was estimated to be approximately 400 km^2 [34]. Equations (3) and (5) give a calculated precursor time, τ_0, and mainshock magnitude, M_p, to be 30.4 yr and 6.3, respectively, assuming that (1) no changes occurred in the far-field tectonic stresses (strains) and (2) the Utsu relationship is applicable to this region. Table 5 lists the seismic events that occurred in the epicentral region beginning with the M2.4 event of 7 June 1961. A seismic search (data provided by the USGS and included all seismic data contained in the Caltech catalogue) in the region 37°N $\rightleftarrows$ 35°N and 118°W $\rightleftarrows$ 119°W for the time period of 1955–1974 shows no events occurred in the epicentral region from 1 January 1955 to 7 June 1961. The data also show that following 11 February 1964, most of the seismic activity developed in the northwest, west, and southern regions that were outside the aftershock region. There was little activity within the aftershock region.

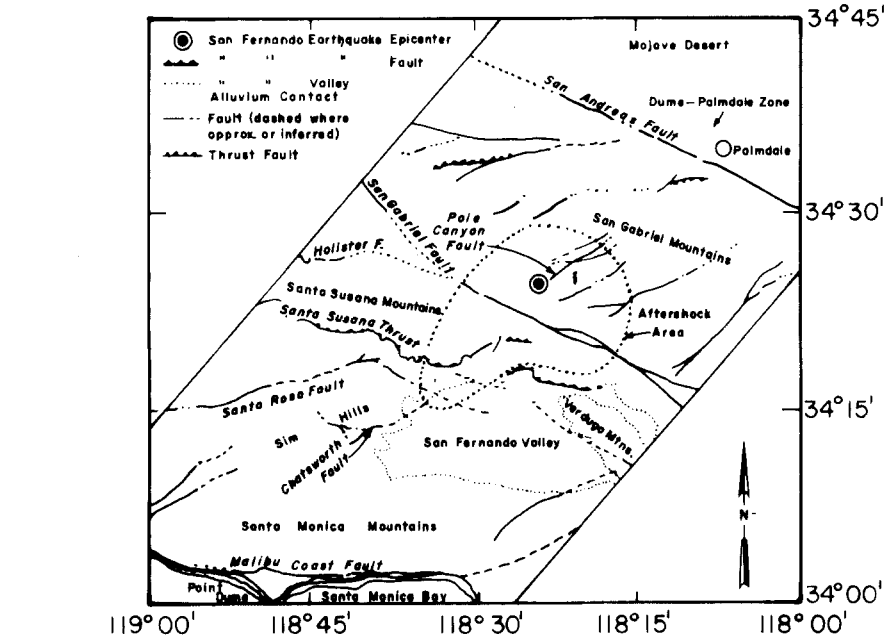

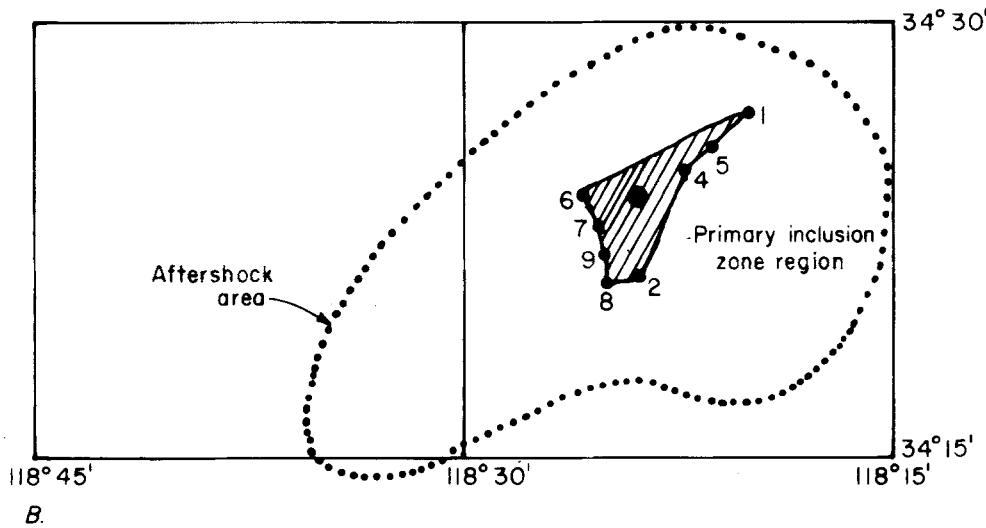

Figure 7

Major tectonic features in the region surrounding the San Fernando mainshock of 9 February 1971, and aftershock area (A) and the hypothesized location of the primary inclusion zone [Fig. 7a is reproduced from reference 5].

Table 5

Seismic events in the epicentral region of the 9 February 1971, San Fernando, California, earthquake

Event	Date	Latitude	Longitude	Magnitude
1*	7 June 1961	34.45°	118.33°	2.4
2*	15 September 1961	34.45°	118.40°	2.0
3	6 October 1961	34.33°	118.48°	3.0
4*	8 December 1961	34.42°	118.37°	2.2
5*	3 February 1962	34.43°	118.35°	2.1
6*	17 March 1962	34.40°	118.43°	2.6
7*	3 May 1962	34.42°	118.38°	2.6
8*	17 September 1963	34.35°	118.41°	2.5
9*	11 February 1964	34.37°	118.40°	2.3
10	9 February 1971	34.40°	118.40°	6.4

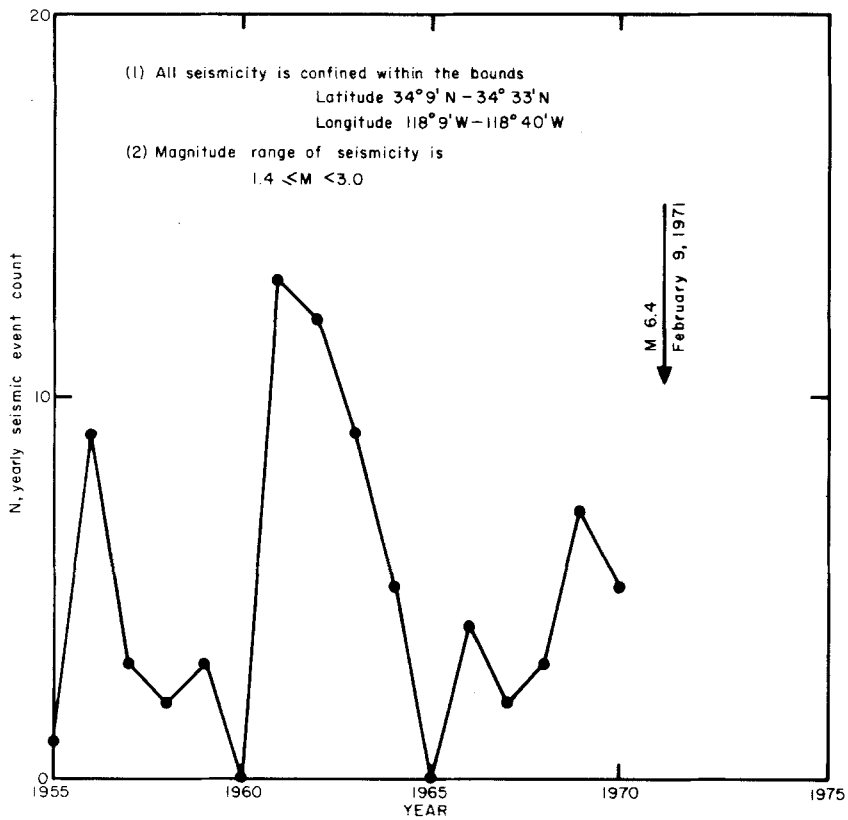

Figure 8
Yearly seismicity count in the San Fernando Region from 1955–1971.

A prediction of the inclusion theory of failure is that the seismicity will increase dramatically as the primary inclusion zone of the impending failure forms and that the seismicity within the area surrounding the primary inclusion zone will decrease once this zone has formed. Figure 8 depicts the yearly seismic event count from 1955 to 9 February 1971. The seismicity examined in this figure was confined to the region 34°9′N ⇄ 34°33′N and 118°9′W ⇄ 118°40′W. Note the pronounced peak in seismic activity beginning in 1961 and terminating early in 1964. This activity was then followed by a slight increase beginning in 1966 and ending in the $M6.4$ mainshock of 9 February 1971. Figure 7b shows the aftershock area and the locations of the seismic events 1 through 9. Thus, the peak of activity during 1961–1964 was primarily associated with the formation of the shaded zone depicted in Fig. 6b.

The data in Figs. 7b and 8 suggest that the primary inclusion zone that gave rise to the $M6.4$ mainshock may have formed between 1961 and 1964. There are additional data supporting this hypothesis. For example, CASTLE *et al.* [13] observed that a major episode of uplift occurred in the epicentral region of the San Fernando mainshock during the 1961–1964 time interval. Such uplift is required when the primary inclusion zone is developing. As the seismic events that form the primary inclusion zone will be characterized by anomalously long rupture lengths, the theory requires that surface displacement will be anomalously large for both the number and magnitude of the seismic events. Thus, the interpretation of the data in Table 5 is consistent with observation. In addition, analysis of the time variation of v_p and v_s [reference 34, Fig. 1b] shows that there is a definite tendency for these velocities to decrease from early 1962. The velocity data are also consistent with the hypothesis that fluids were present within the focal volume. Once the primary inclusion zone has formed, the fluids will be expelled from the focal region of the impending mainshock. Thus, at shallow depths the cracks in the focal region will expand and the cracks will become undersaturated. The compressional velocity, v_p, and to a lesser extent, the shear velocity, v_s, will decrease at this point because of the high compressibility of the rock containing dry or unsaturated cracks. Once the crack closure front has passed, the velocity anomalies will disappear. Consequently, the velocity anomalies can be interpreted as being consistent with the hypothesis that the primary inclusion zone formed in the 1961–1964 time interval and that this zone developed within a region that was fluid saturated.

The calculated time, τ_{d0}, to form the primary inclusion zone is found from equation (C.5) to be approximately 22 months, using the observed mainshock magnitude of $M6.4$. The seismic events 1 through 9 in Table 5 give an observed time duration of nearly 32 months (2.6 yr) required to form this zone. Seismic event 3, of magnitude $M3$, in Table 5 has been excluded from representing part of the primary inclusion zone. Thus, the seismic events hypothesized to have formed the zone are all in magnitude range of 2.0 to 2.6. It is of interest to note that the number of events, 8 in total, compares favorably with the predicted value of 10 (equation (16)).

The area of the hypothesized primary inclusion zone in Fig. 7b is approximately

40 km^2. The calculated value is $A_i = \tau_{d0}/\alpha = 33$ km^2, where $\alpha = 2.43 \times 10^{-4}$, using the 'observed' value of $\tau_d = 31$ months. The precursor time for the mainshock was reduced nearly 300% from 30 yr to approximately 10 yr. This result suggests, not surprisingly, that changes are developing in the far-field boundary conditions during the time duration (τ_0) required for the mainshock to develop. Equation (26) gives the corrected precursor time–focal region area for earthquakes of comparable magnitude in this region, assuming the boundary conditions change in the same prescribed manner to be $\tau = 5.70 \times 10^{-5} A$, where τ and A are measured in seconds and square centimeters, respectively.

The formation of the primary inclusion zone of an impending shock of magnitude M was shown earlier to be represented by a decrease in gravitational potential energy of amount Ψ_p (equation (19)). This process occurs over a time interval during which the far-field tectonic stresses can be assumed constant. Thus, the energy decrease, Ψ_p, must be manifested by a corresponding increase of gravitational potential energy in the region surrounding the primary inclusion zone. For the San Fernando shock, equation (19) gives Ψ_p to be approximately 6.30×10^{23} ergs. This energy compares with the energy of 2.5×10^{21} ergs radiated by the mainshock and is sufficient to vertically displace a volume of rock, V, by an amount $\Psi_p/\rho V g$, where ρ is mass density, g, the gravitational constant (10^3 cm/sec^2). Let V be Ah, where A and h denote the vertical thickness and A the cross-sectional area of the rock mass. If $A \sim 20{,}000$ km^2, $h \sim 10$ km, then $\delta h \sim 1.50$ cm for $\rho = 3.5$ g/cm^3. Thus, the theory predicts that anomalous uplift should be associated with the formation of the primary inclusion zone of an impending shock, and further, the greatest rate of uplift will occur during the time interval τ_d ($\sim$31 months for the San Fernando earthquake). The above calculations are consistent with recent observations reported by CASTLE *et al.* [52] on the uplift in the Palmdale–Dume region, near the epicentral region of the 1971 San Fernando shock. An estimate of the average stress increase, $\delta\sigma$, associated with the formation of the primary inclusion zone of the 1971 shock, assuming the uplift is 'elastic' is $\delta\sigma \sim (\delta h/h)E_0/\nu_0 \sim 9$ bars, where E_0 and ν_0 are taken to be 1×10^{12} dynes/cm^2 and 0.30, respectively. These order of magnitude calculations are suggestive that the observed uplift (covering approximately 12,000 km^2 [51]), while being of a tectonic nature, should not be confused with the processes leading to an impending earthquake, rather, the result of physical processes that led to the formation of the San Fernando mainshock on 9 February 1971. If event 9 in Table 5 marks the termination of the primary inclusion phase, then v_p and v_s should begin to decrease in the focal region as fluids diffuse away from the primary inclusion zone. This behavior would be evidenced by earthquakes in the focal volume tending to migrate with time away from the primary inclusion zone. This behavior is observed. Lastly, the predicted minimum dimension of the anomalous region, assuming an average maximum 'background' seismicity of $M_{\max} = 2.5$, is 125 km, respectively. This value compares favorably with the value of 80 km quoted by WHITCOMB *et al.* [34].

The August 1973, earthquake at Blue Mountain Lake, New York

A magnitude $M2.6$ earthquake occurred at Blue Mountain Lake at a depth of approximately 1 km on 3 August 1973. This earthquake was preceded by approximately 5 days by decreases in v_p and v_s of approximately 22% and 12% below normal. The anomalous zone (region of low v_p) for this earthquake was about 3 km → 5 km radius. According to AGGARWAL *et al.* [2], the anomalous zone had a radius of at least 6, but probably less than 10 times the radius of the aftershock zone. AGGARWAL *et al.* [2] observed that the *P*-wave delays were a maximum in the hypocentral region of the earthquake and decreased away from this region. The earthquake occurred approximately one day following a return of v_p/v_s to its pre-anomaly value. Both these results are consistent with the existence of pore fluids within the focal volume of this earthquake for reasons discussed earlier in this article.

The aftershocks of this event were observed to occur within an elliptically shaped zone whose dimensions were slightly less than 1 km by 0.3 km, giving an aftershock area of 0.24 km^2. Equation (3) gives a calculated precursor time, τ_0, for this event of approximately 6.8 d. The observed time, measured from the onset v_p/v_s decrease, was approximately 5 d. Note that the time of onset of the v_p/v_s decrease must be considered to represent a *minimum* value for τ_0. The average maximum magnitude of the background seismicity, $M_{\max}$, in this region is approximately 1.0 [1, 2], giving a calculated minimum diameter of the anomalous volume of approximately 22 km. These values are well within the bounds calculated by AGGARWAL *et al.* [2]. AGGARWAL *et al.* also observed that the future rupture zone was seismically quiet during the time of the low v_p/v_s values preceding the 3 August event. Nearly all the seismic events studied occurred in an area surrounding the aftershock zone. This result is in agreement with the behavior predicted by the inclusion theory. However, the calculated magnitude of the 3 August shock, assuming that the aftershock area (A) magnitude (M) satisfies the Utsu relationship is $M3.1$, a discrepancy in magnitude of nearly 0.5. This result may possibly be interpreted as indicating that pore fluids were present within the hypocentral region of the 3 August event. The magnitude of this pressure is found from equation (28) to be approximately $0.60\sigma_3$, where σ_3 for this event is the vertical stress and is approximately 0.2 kb. Thus, P_f in the hypocentral region of the 3 August shock is predicted to be in the order of 0.12 kb.

The 3 October and 9 November 1974, Peru earthquake sequence

An earthquake sequence that may have important seismological and sociological implications occurred approximately 60 km off the coast of central Peru between 3 October and 9 November 1974 and within a well-documented seismic gap. The 3 October ($m_b = 6.3$, $M_s = 7.6$, USGS) and 9 November ($m_b = 6.0$, $M_s = 7.2$, USGS) shocks were shallow (~ 20 km depth), complex multiple ruptures that began with a low energy episode followed by higher energy ruptures [30]. The subsequent

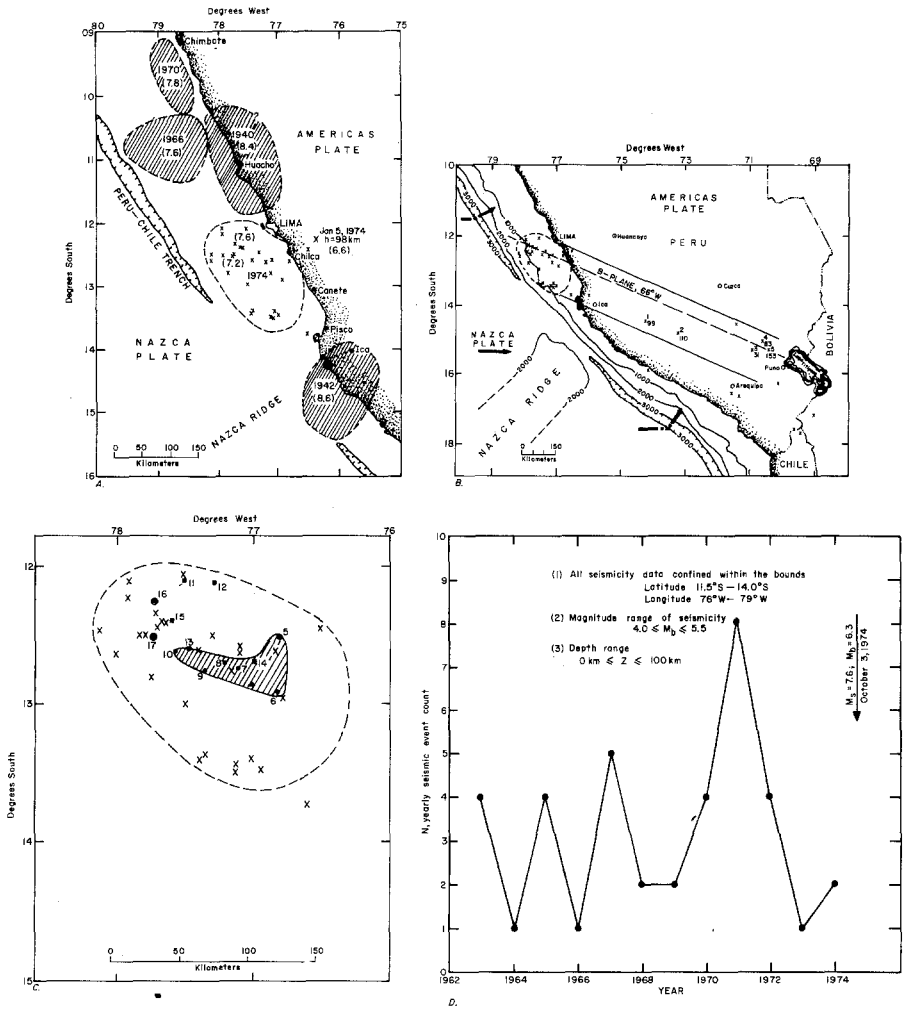

Figure 9

Location of mainshock and aftershock region of the 3 October–9 November 1974 Peru earthquake sequence. A. Relationship of 3 October 1974 aftershock region to previous earthquakes in the immediate epicentral region. B. Rupture propagation direction of the 3 October mainshock. C. Location and dimensions of the hypothesized primary inclusion zone of the 3 October mainshock. D. Yearly seismicity count versus time in the epicentral region of the 3 October–9 November mainshocks. [Figures A–B are reproduced with permission of SPENCE and LANGER, 1975].

aftershock sequence of the 3 October event, occurring within an elliptical zone some 250 km by 150 km, partially filled the seismic gap and was essentially terminated by the 9 November 1974 mainshock (Figs. 9a,b). The primary aftershock region of the 3 October event since 14 November 1974 is now very near to the normal background level of seismic activity. Subsequent activity has shifted to the north-northeast of this region [SPENCE, personal communication, 1975].

Table 6

Precursory seismicity in the immediate epicentral region prior to the 3 October–9 November 1974, Peru earthquake sequence
(after SPENCE and LANGER, 1976)

Date	Latitude °S	Longitude °W	Depth (km)	m_b	M_s
1. 7 October 1963	12.9	76.8	69	5.4	—
2. 22 August 1967	12.5	76.8	57	4.8	—
3. 5 August 1968	12.8	76.8	78	4.4	—
4. 9 February 1970	12.8	77.2	40	4.6	—
*5. 28 May 1971	12.5	67.8	56	4.9	—
*6. 1 August 1971	12.9	76.8	64	5.2	—
*7. 1 October 1971	12.8	77.1	43	4.7	—
*8. 3 October 1971	12.7	77.2	—	4.6	—
*9. 3 October 1971	12.8	77.4	42	5.2	—
*10. 3 October 1971	12.6	77.6	—	4.2	—
*11. 19 June 1972	12.1	77.5	72 (?)	5.2	—
*12. 29 January 1973	12.1	77.3	63	4.5	—
*13. 24 December 1973	12.6	77.5	—	5.4	—
*14. 31 August 1974	12.7	77.0	61	4.4	—
*15. 27 September 1974	12.4	77.6	41	5.0	—
16. 3 October 1974	12.3	77.7	20	6.3	7.6
17. 10 October 1974	12.4	77.6	27	5.3 (largest aftershock)	—
18. 9 November 1974	12.5	77.7	10	6.0	7.2
19. 14 November 1974	12.8	77.1	shallow	5.4	—

Table 6 summarizes the date, focal depth, and magnitude data for the seismic events that preceded the 3 October 1974 event. Location accuracy of these events is ± 15 km [SPENCE, personal communication, 1975]. These data show that no seismic event occurred in the immediate hypocentral zone between 1962 and 1970. The precursory seismicity data, however, suggest a peak of activity on 3 October 1971, followed by a period of relative quiescence in the epicentral region. Seismic events 5 through 10, beginning on 28 May and terminating on 3 October 1971, a time span of approximately 4 months, map out an area, A_i, of approximately 1.5×10^{13} cm^2. These events migrated in time toward the epicentral regions of the 3 October and 9 November shocks, and as such, appear to be causally related to these shocks. There was *no* further activity within this zone until the mainshock of 3 October 1974. It should be noted that events 1–4 developed within the E–SE portions of this zone several years prior to, and may have been instrumental in, its formation.

Figure 9d illustrates the yearly seismic event count within the bounds 11.5°S $\rightleftarrows$ 14.0°S and 76°W $\rightleftarrows$ 79°W. The body-wave magnitude range of the seismicity in this figure is $4.0 \leq m_b \leq 5.5$. Note the pronounced peak in seismic activity that occurred during 1971, followed by a period of relative quiescence that terminated with the 3 October 1974 mainshock. Figure 9c shows the aftershock area and the locations of

seismic events 5 through 15. The peak of seismic activity in 1971, like the peak of seismic activity associated in the San Fernando region and the rockburst discussed earlier, was associated with the formation of the shaded zone depicted in Fig. 9c. Thus, the data in Figs. 9c,d suggest that the primary inclusion zone associated with the 3 October 1974 mainshock may have formed during the time interval between 28 May 1971 and 3 October 1971.

The 3 October and 9 November shocks occurred within a well-documented seismic gap that is of a size to suggest that it could have supported a much larger magnitude earthquake sequence than what did actually occur (Fig. 9a). There is also some seismic evidence that suggests that the earthquakes in the sequence were 'anomalous' events in that the actual shock could have been of a much larger magnitude ($\leq M8$). The estimated aftershock area, A, of the 3 October 1974 event was approximately 3.0×10^{14} cm^2 [30]. The calculated magnitude of an event having an aftershock area of this dimension is calculated from equation (5) to be approximately $M_p8.2$, where it is assumed that the modified Utsu relationship between A and M_p is applicable to this region. If the seismic event sequence ($5 \rightarrow 10$) in Table 6 can be assumed to denote the formation of the primary inclusion zone of this shock, then the calculated aftershock area A ($A = 21.8A_i$), of this event is approximately 3.3×10^{14} cm^2, in good agreement with the observed aftershock area. The class I precursor time, τ_0, for the calculated mainshock ($M_p8.2$) and the time, τ_{d0}, required to form the primary inclusion zone of this event would have been 2405 yr and 113 yr, respectively, in the *unlikely* situation of there being no changes in the far-field boundary conditions due, for example, to plate motions during the time τ_0 and the predicted time required to form the primary inclusion zone. Thus, assuming that (1) the Utsu relationship is applicable to this region and (2) the time, τ_d, to form the inclusion zone required only 4 months, the calculated time to the mainshock becomes $\tau = \tau_0(\tau_d/\tau_{d0}) = 7.1$ yr, a reduction from the theoretical value by a factor of nearly 300. Substituting these values into (26) gives a predicted velocity, v, at which changes are occurring in the far-field boundary conditions equal to 28 km/yr. This value is in close agreement with observational and theoretical treatments of the average velocity of strain pulses in the lithosphere along major subduction zones [8, 45, 46].

The calculated precursor time for an event of this magnitude ($M_p8.2$) would have required approximately 7 yr. This time is measured from the 28 May 1971 event. However, the actual earthquake sequence occurred 3 yr from that time. The observed partial filling of the aftershock region of the 3 October 1974 mainshock could be interpreted as indicating that this region may not have had the time required for the preparation of the larger magnitude shock. In addition, it should be noted that events 11, 14, and 15 (Table 6) occurred within the epicentral region of the 3 October and 9 November mainshocks. In particular, events 13, 14, and 15 appear to migrate toward the hypocenters of these shocks. These events were of significant magnitude to have acted as possible 'destressing earthquakes' in the region of what could have been a magnitude $M8.2$ shock. Destressing serves to produce smaller failures, where

only a large failure could have occurred in the absence of destressing. Similar behavior has been reported to occur in mines experiencing rockbursts [12]. It is conceivable, therefore, that both the 3 October and 9 November shocks may have been 'triggered' by events 11, 14, and 15. Thus, according to these arguments, it is theoretically possible that the mainshock should have been much larger (M8.2) than what was actually observed (M_s7.6).

There is some evidence that suggests this region may have again approached a critical state. For example, the multiple rupture characteristics of the 3 October and 9 November events, taken in context of the inclusion theory, may signify a low compression level of the least local principal stress in the hypocentral region. Similarly, the relatively high M_s values of these events may be an indication that this stress is nearing or has attained a tensile value in the hypocentral region. Necessary and sufficient conditions for an impending failure include the condition that σ_3 become tensile within the inclusion zone. As discussed above and elsewhere [11, 12], destressing seismic events, such as may have occurred in events 13, 14, and 15, merely postpone the total release of the energy that is stored in the region. In addition, the magnitude of the event that may occur, assuming no additional destressing-type events occur during the earthquake preparation process, may be larger than the event that would have occurred had the destressing shocks not occurred, that is, the magnitude of the impending shock will be at least M8.2, and possibly higher.

These arguments and the observational data that the 9 November 1971 shock terminated the earthquake sequence with only one additional aftershock (event 19, Table 6) nearly 5 days later are consistent with the theoretical conditions discussed earlier in this article that this region may now be in the process of being prepared for an earthquake whose magnitude will be at least M8.2. The 14 November 1974 shallow focus event occurred within and near the eastern end portions of the zone that may have been the postulated primary inclusion zone of the 3 October and 9 November mainshocks. According to SPENCE [personal communication, 1975], this shock produced a radiation pattern characteristic of deep earthquakes, that is, small rupture length but high energy release. Thus, the location of the 14 November event may mark the eastern termination of the inclusion zone of the impending mainshock.

If the hypocentral regions affected by the 3 October and 9 November events are now contained within this inclusion zone, then the total area of the 'new' primary inclusion zone is of the order of 3×10^{13} cm^2. The *predicted* magnitude and class I precursor time, τ, is measured from the 14 November 1974 event. However, without more reliable information on the dimensions of the hypothesized new primary inclusion zone, the best estimate that can be made at this time of the magnitude of the impending shock is that it will be at least M8.2. Accordingly, if there are no further destressing seismic events and the far-field boundary conditions in this region change in the same prescribed manner as for the 3 October 1974 shock, then the predicted class I precursor times for a range of predicted magnitudes of 8.2, 8.3, and 8.5 are

7.1 yr, 8.9 yr, and 14 yr, respectively. The predicted location and preferred fault plane for this event should be similar to those of the 3 October 1974 shock (Fig. 9b). This earthquake, like the 3 October–9 November 1975 sequence, will be an underthrust event.

In this interpretation of the Peru sequence, I have assumed that the Utsu relationship is applicable to this region. Thus, the anomalously large size of the aftershock region for the 3 October 1974 event and the relatively small magnitude ($m_b = 6.3$, $M_s = 7.6$) of the earthquake that produced the aftershock region may be evidence that the region may not have been relieved of the available stored energy. However, as discussed earlier in the text, it is possible that the existence of fluids under pressure in the hypocentral region of the 3 October shock may be partially responsible for lowering the 'predicted' magnitude, based on the observed aftershock area, from 8.2 to 7.6. Yet, neighboring regions, such as shown in Fig. 9a, have also experienced great earthquakes ($\geq M8$) in the recent past. Thus, there is no obvious reason to assume that the epicentral region of the 3 October 1974 event is any different. Similarly, historical records indicate that this region has experienced large earthquakes (and their accompanying tsunamis) in the historical past (28 October 1746; $M \sim 8.4$, SPENCE and LANGER, personal communication, 1976).

The hypothesis that the primary inclusion zone of an impending great earthquake may have formed approximately 75 km off the coast of central Peru on 9 November 1974 can be tested by detailed monitoring of sea level changes (sea level should decrease as the focal region begins to store energy), anomalous v_p, v_s, and/or v_p/v_s behavior if fluids are present in the focal region, radon emanations, possible secular variations in the geomagnetic field, and other class I precursors that have been reportedly observed prior to major earthquakes. If the measurements support this interpretation, then detailed monitoring of the region for the class II type precursor is in order. Detection of the class II precursors may give a few hours warning of the impending shock.

Discussion

Theoretical arguments and supporting data presented in this article suggest that the inclusion theory of failure and its associated scale invariant properties may have important applications to earthquake seismology and, in particular, to the problem of earthquake prediction. It was shown that to have a predictive capability, detailed knowledge of both when the primary inclusion forms and its geometrical characteristics are essential. Knowledge of the dimensions of the primary inclusion zone and the time duration required for its formation provides an estimate of both the magnitude and the class I precursor time for the impending failure. In addition, it was shown that there are features characteristic of earthquake prone regions which indicate that accurate prediction of both the class I precursor time and the magnitude of an

impending earthquake is difficult. Changes in the far-field tectonic boundary conditions due, for example, to plate motions occurring during the normal class I precursor time interval as well as the existence of pore fluids under pressure in the focal volume of an impending shock are both factors that influence the precursor time–magnitude relationship. However, once it has been determined how these parameters affect the class I precursor time–focal region area–magnitude relationships in a given region, then it is possible to adjust the theoretical relationships so as to accurately predict these parameters for other earthquakes in the same region, *providing*, of course, that the boundary conditions change in the same prescribed manner. These difficulties, however, do not arise for the class II precursors since their time durations are short enough that changes in the far-field boundary conditions are, for all practical purposes, constant during the class II time duration. Thus, monitoring of this precursor class in the epicentral region of an impending earthquake may provide an accurate indicator of when the mainshock will occur.

The criteria required to determine when a region is approaching or has approached a condition that it will experience an earthquake are readily provided by the inclusion theory. These criteria include the following: (1) A determination of the b-value variation of the seismic events occurring within the anomalous (or dilated) volume. The b-values are predicted to decrease as the deformation band, within the primary inclusion zone will form, develops within the anomalous volume. (2) Once a candidate region has been found, detailed monitoring of this region is required to determine where and when the primary inclusion zone forms. The events that form this zone are predicted to be relatively few in number (≤ 10). Each event will be characterized by anomalously large rupture lengths since they are forming within a stress field characterized by a tensile value of the local least principal stress. The b-values of these events are predicted to be low. In addition, since these events are predicted to have long rupture lengths, anomalous uplift and/or anomalous horizontal expansion, depending upon the focal mechanism of the impending mainshock, both within and outside the epicentral region are predicted. The overall level of background seismicity will decrease once the primary inclusion has formed. (3) The epicentral region of the impending earthquake should be instrumented at this time so as to detect the onset of the class II precursor.

It is of particular importance to note that the numerical calculations, such as the energy budget of a failure, that have been performed in this article are subject to revision as more reliable data on the functional relationship between the aftershock area and magnitude are available. This relationship may be dependent upon the location and physical characteristics of the rock materials in the focal volume. *This relationship represents the 'calibration factor' in applying the inclusion theory to given earthquake prone zones.*

It should also be clearly understood that the inclusion theory is directly applicable to failures along existing fault zones as the physical processes reponsible for 'lock zone' failure and 'fresh' failures are identical. However, when applying the theory

to the prediction of earthquakes along existing fault zones, it is possible that considerable underestimation of the magnitude of an impending shock, even when factors due to pore fluids have been taken into account, can result since failure of the lock zone may *also* result in the sudden release of stored strain energy along the fault zone outside the lock point. *Thus, it is theoretically possible that a large magnitude shock could occur only when a much smaller magnitude shock has been predicted.* We have found evidence supporting this prediction from certain classes of rockbursts in northern Idaho, that is, rockbursts that develop along pre-existing fault zones that are activated by mining.

The inclusion theory requires the existence of low magnitude foreshocks, termed primary foreshocks, whose magnitudes are approximately $M-5.3$, where M is the mainshock magnitude, to form in the hypocentral region during the time duration of the class II precursor phase. This class of foreshocks should not be confused with secondary foreshocks which may occur in the focal volume of the mainshock as a result of strength variations in the rock mass comprising the focal volume. Secondary foreshocks can serve to prematurely 'trigger' the mainshock. It is to be noted that the spectral characteristics of secondary foreshocks will be considerably different than primary foreshocks for reasons discussed earlier in the text. It is also important to note that the inclusion theory requires that the probability of occurrence of secondary foreshocks will increase as the magnitude of the mainshock increases. The reason for this behavior is that as the size of the primary inclusion zone increases, the greater the probability that this region will include rock materials of greater strength disparity. Thus, as the focal region of the impending shock approaches a critical state, that part of the primary inclusion zone containing rock of the lowest strength will fail first. Failure of this zone will then load the adjacent stronger region and thereby trigger the mainshock.

Lastly, it is of interest to observe that the deviation of the observed class I precursor time, τ, from the predicted time, τ_0, which is obtained when no changes are occurring in the far-field boundary conditions must provide a relative indication of how the boundary conditions that indirectly produce the earthquake are changing in the region where the earthquake is occurring. Thus, the deviation of τ_0 and τ in Fig. 5 should provide quantitative information of relative plate velocities, or alternatively, the relative magnitude of how the far-field strains induced within a given earthquake prone region are changing in response to these relative plate motions. Evidence presented in this article lends support to this hypothesis. Clearly, this aspect of the earthquake problem warrants further attention.

Acknowledgments

William Spence kindly provided me a preprint of his results on the 3 October and 9 November 1974 Peru earthquake sequence. Discussions with Dr. Spence on this

sequence are gratefully acknowledged. In addition, I would like to extend my appreciation to Max Wyss and the anonymous reviewers of this sequence of papers. Their conscientious reviews have been of considerable value to me in improving the final manuscripts.

References

[1] Y. P. Aggarwal, L. R. Sykes, J. Armbruster, and M. L. Sbar (1973), *Premonitory changes in seismic velocities and prediction of earthquakes,* Nature, *241*, 101–104.

[2] Y. P. Aggarwal, L. R. Sykes, D. W. Simpson, and P. G. Richards (1975), *Spatial and temporal variations in τ_s/τ_p and in P-wave residuals at Blue Mountain Lake, New York: application to earthquake prediction,* J. Geophys. Res. *80*, No. 5, 718–732.

[3] D. L. Anderson and J. H. Whitcomb (1975), *Time-dependent seismology*, J. Geophys. Res. *80*, No. 11, 1497–1503.

[4] C. Archambeau and S. Sammis (1970), *Seismic radiation from explosions in prestressed media and the measurement of tectonic stress in the earth*, Rev. of Geophys. Space Phys. *8*, No. 3, 473–499.

[5] M. Båth, *Handbook on Earthquake Magnitude Determinations* (Seismological Institute, Uppsala, Sweden, 1969), 158 pp.

[6] B. T. Brady (1974), *Theory of earthquakes—I. A scale independent theory of failure*, Pure appl. Geophys. *112*, 701–726.

[7] B. T. Brady (1975), *Theory of earthquakes—II. Inclusion theory of crustal earthquakes*, Pure appl. Geophys. *113*, 149–169.

[8] B. T. Brady (1976), *Theory of earthquakes—III. Inclusion theory of deep earthquakes*, Pure appl. Geophys. *114*, 119–139.

[9] B. T. Brady (1976), *Laboratory investigation of tilt and seismicity anomalies in rock before failure*, Nature, *260*, No. 5547, 108–111.

[10] B. T. Brady (1976), *Dynamics of fault growth: A physical basis for aftershock sequences,* Pure appl. Geophys. (in press).

[11] B. T. Brady (1975), *Seismic precursors prior to rock failures in underground mines,* Nature *252*, 549–552.

[12] B. T. Brady and F. W. Leighton (1976), *Seismicity anomaly prior to a moderate rock burst: A case study,* to be presented and published in the *Proceedings of the 17th Rock Mechanics Symposium, Snowbird, Utah, August 25–27, 1976.*

[13] R. L. Castle, J. N. Alt, J. C. Savage, and E. J. Balaza (1974), *Elevation changes preceding the San Fernando earthquake of February 9, 1971*, Geology *2*, 61–66.

[14] W. L. Ellsworth (1975), *Bear Valley, California, earthquake sequence of February–March, 1972*, Bill. Seis. Soc. Am. *65*, No. 2, 483–586.

[15] T. C. Hanks (1974), *Constraints on the dilatancy–diffusion model of the earthquake mechanism*, J. Geophys. Res. *79*, No. 20, 3021–3025.

[16] J. Kelleher and J. Savino (1975), *Distribution of seismicity before large strike-slip and thrust-type earthquakes*, J. Geophys. Res. *80*, No. 2, 260–271.

[17] A. McGarr (1971), *Violent deformation of rock near deep-level, tabular excavations—Seismic events*, Bull. Seism. Soc. Amer. *61*, No. 5, 1453–1466.

[18] K. Mogi (1968), *Development of aftershock areas of great earthquakes*, Bull. Earthquake Res. Inst. *46*, 175–203.

[19] I. L. Nersesov, A. A. Lukk, V. S. Ponomarev, T. G. Rautain, B. G. Rulev, A. N. Semenov, and I. G. Simbireva, *Possibilities of Earthquake Prediction, Exemplified by the Garm Area of the Tadzhik, S.S.R., in Earthquake Precursors*, ed. M. A. Sadovskii, I. L. Nersesov, and L. G. Latynina (Academy of Science of the USSR, Moscow, 1975), pp. 79–99.

[20] J. C. Jaeger, *Elasticity, Fracture and Flow* (2nd Ed.) (John Wiley and Sons, New York, 1962).

[21] R. J. O'Connell and B. Budiansky (1974), *Seismic velocities in dry and saturated cracked solids*, J. Geophys. Res. *79*, No. 35, 5412–5426.

[22] L. OBERT and W. I. DUVALL, *Rock Mechanics and the Design of Structures in Rock* (John Wiley and Sons, New York, 1968), 650 pp.
[23] E. OROWAN (1938), *The mechanical strength properties and the real structure of crystals*, Z. Kristallographie *89*, 327–343.
[24] H. F. REID (1911), *The elastic rebound theory of earthquakes*, Bull. Dept. Geol., Univ. of Calif. *6*.
[25] N. J. PETCH, *Metallographic aspects of fracture*, in *Fracture: An Advanced Treatise* (ed. H. Llebowitz) (Academic Press, 1968), pp. 351–390.
[26] F. PRESS and C. ARCHAMBEAU (1962), *Release of tectonic strain by underground nuclear explosions*, J. Geophys. Res. *67*, No. 2, 335–343.
[27] R. A. SACK (1946), *Extension of Griffith's theory of rupture to three dimensions*, Proc. Phys. Soc., Lon. *58*, 729–736.
[28] K. SASSA (1944), *Tilting motion of ground observed before and after the destructive Tottori earthquake, Kagaku*, Science *14*, No. 6, 220–221.
[29] K. SASSA and E. NISHMURA (1951), *On phenomena forerunning earthquakes*, Trans. Amer. Geophys. Union *32*, No. 1, 1–6.
[30] W. C. SPENCE, C. J. LAGER, and J. N. JORDAN, *A tectonic study of the Peru earthquakes of October3 and November 9, 1974* (in preparation).
[31] T. UTSU and A. SEKI (1955), *A relation between the area of the aftershock region and the radius of the sensibility circle* (in Japanese), Zisin *3*, No. 34, 1955.
[32] J. B. WALSH (1968), *Mechanics of strike-slip faulting with friction*, J. Geophys. Res. *73*, No. 2, 761–776.
[33] R. WESSON and W. ELLSWORTH (1973), *Seismicity preceding moderate earthquakes in California*, J. Geophys. Res. *78*, 8527–8546.
[34] J. WHITCOMB, J. GARMANY, and D. L. ANDERSON (1973), *Earthquake prediction: Variation and seismic velocities before the San Fernando earthquake*, Science *180*, 632–635.
[35] M. WYSS (1975), *Precursors to the Garm earthquake of March 1969*, J. Geophys. Res. *80*, No. 20, 2926–2930.
[36] T. MATUZAWA, *Study of Earthquakes* (UNO Shoten, Tokyo, Japan, 1964), 213 pp.
[37] T. UTSU (1969), *Aftershocks and earthquake statistics (I)*, J. Fac. Sci., Hokkaido Univ. Ser. *73*, 129–195.
[38] T. HAGIWARA and T. RIKITAKI (1967), *Japanese program on earthquake prediction*, Science *157*, 761–762.
[39] A. M. KONDRATENKO and I. L. NERSESOV (1962), *Some results of a study of changes in the speeds of longitudinal and transverse waves in the focal zone, physics of earthquakes and explosion seismology*, Tr. Inst. Fiz., Zomli Akad. Nauk, USSR, *25*.
[40] J. B. SMALL and E. J. PARKIN, *Horizontal and Vertical Crustal Movement in the Prince William Sound, Alaska, Earthquake of 1964*, paper presented to the Fifth United Nations Regional Cartographic Conference for Asia and the Far East, Canberra, Washington, E.S.S.A., U.S. Dept. of Commerce, March 1967.
[41] A. E. OSTROVSKY, *Long-Period Waves and Tilts of the Earth's Surface Before Strong Earthquakes* (abstract) (International Union of Geodesy and Geophysics, Grenoble, 1975).
[42] M. WYSS (1974), *Will there be a large earthquake in Central California during the next two decades?* Nature *251*, 126–128.
[43] R. ROBINSON, R. L. WESSON, and W. L. ELLSWORTH (1974), *Variation of P-wave velocity before the Bear Valley, California, earthquake of February 24, 1972*, Science *184*, 1281–1283.
[44] V. I. MJACHKIN, W. F. BRACE, G. A. SOBOLEV, and J. H. DIETERICH (1974), *Two models for earthquake forerunners*, Pure appl. Geophys. *113*, No. 1/2, 169–183.
[45] K. MOGI (1973), *Relationship between shallow and deep seismicity in the Western Pacific region*, Tectonophysics *17*, 1–22.
[46] T. RIKITAKE (1975), *Earthquake precursors*, Bull. Seismo. Soc. Amer. *65*, No. 5, 1133–1162.
[47] F. R. GORDON (1970), *Water level changes preceding the Meckering, Western Australia, earthquake of October 14, 1968*, Bull. Seismo. Soc. Amer. *60*, No. 5, 1739–1740.
[48] W. D. STUART (1974), *Diffusionless dilatancy model for earthquake precursors*, Geophys. Res. Let. *1*, 261–264.
[49] F. D. STACEY, *Physics of the Earth* (John Wiley and Sons, Inc., New York, 1969).

[50] C. F. RICHTER, *Elementary Seismology* (Freeman and Sons, San Francisco, 1958).
[51] J. H. WHITCOMB, C. A. ALLEN, J. D. GARMANY, and J. A. HILEMAN (1973), *The February 9, 1971 San Fernando earthquakes and aftershocks*, Rev. Geophys.
[52] R. O. CASTLE, J. P. CHURCH, and M. R. ELLIOTT (1976), *Aseismic uplift in Southern California*, Science *192*, 251–253.
[53] T. UTSU (1969), *Aftershocks and Earthquake Statistics (I)*, J. Fac. Sci., Hokkaido Univ. Ser. *73*, 129–195.

(Received 22nd December 1975)

Appendix A

Glossary of Terms and Symbols

Terms

(1) *Anomalous Zone*: This zone refers to the dilation zone within which a deformation band will form prior to a major failure.
(2) *Deformation Band*: This band denotes the portion of the anomalous zone within which the principal stress axes rotate as the region is being prepared for a major failure.
(3) *Primary Inclusion Zone*: This zone forms within the deformation band at a time prior to failure that is dependent on the magnitude of the failure that will occur. The formation of this zone marks the initiation of the class I precursor phase.
(4) *Secondary Inclusion Zone*: This zone represents the inclusion from which secondary crack growth occurs within the primary inclusion zone. This crack growth leads to the coalescence of cracks within the primary inclusion to form the macrocrack. The formation of this zone marks the initiation of the class II precursor phase.
(5) *Tertiary Inclusion Zone*: This zone denotes the inclusion from which macrocrack growth occurs during the growth phase of the mainshock. The formation of this zone marks the initiation of the class III precursor phase.
(6) *Macrocrack Zone*: The zone containing the macrocrack within the primary inclusion zone.
(7) *Focal Region*: The region into which the failure is propagated. This region

represents the zone where strain energy storage occurs during the preparation stage of the mainshock and where the aftershocks occur.

(8) *Hypocenter*: The contact between the fault zone and the primary inclusion zone. The hypocenter denotes the location where closure of the macrocrack first occurs.

(9) *Fault Zone*: Represents the faulted region that precedes the primary inclusion zone. The fault represents that part of the macrocrack that has closed.

(10) *Lock Point Zone*: A zone along a pre-existing fault zone where movement is prohibited. This zone represents the region within which a primary inclusion that will lead to its failure is nucleated.

Symbols

σ_{10}, σ_{30}	Far-field maximum (σ_{10}) and least (σ_{30}) principal stresses. These represent the principal stresses that exist outside and are far removed from the anomalous region within which the mainshock occurs.
σ_1, σ_3	Local values of the maximum and least principal stresses within the deformation band.
θ	The angle between σ_{10} and σ_1.
σ_c, σ_t	Principal stresses parallel (σ_c) and normal (σ_t) to the major axis of the primary inclusion zone.
σ_{t0}	The magnitude of σ_t at the inception of failure.
$\sigma_d\ (=\sigma_1 - \sigma_3)$	Principal stress difference within the focal region.
σ_c^*, σ_t^*	Compressive and tensile stresses existing in the region outside the macrocrack zone during the time duration of the class II precursor.
v_p, v_s	Longitudinal and transverse wave velocities.
L_i, A_i	Length and area of the primary inclusion zone.
L, A	Average dimension and area of the focal region of the primary inclusion zone.
A_c	Area of the average-sized cracks within the primary inclusion zone.
l_c	Fundamental inclusion length ($\sim 10^{-7}$ cm).
τ_0, τ	Predicted and observed times of the class I precursor.
τ_{s0}, τ_s	Predicted and observed times of the class II precursor.
τ_{r0}, τ_r	Predicted and observed times of the class III precursor.
τ_{d0}, τ_d	Predicted and observed times required to form the primary inclusion zone.
$v_0\ (=L/\tau_0)$, $v\ (=L/\tau)$	Average predicted and average observed velocity of the crack closure front in the focal region of the primary inclusion zone.

l_0	Average linear dimension of the deformation band. This length also denotes the average minimum dimension of the anomalous zone.
M_p, M	Predicted and observed magnitudes of the mainshock.
$M_{\max}$	Predicted background value of the average maximum magnitude of seismic events within the anomalous zone.
Ψ_0, Ψ	Total potential energy changes of the system due to presence of the primary inclusion zone when fluids are not present (Ψ_0) or present (Ψ) in the focal volume of the primary inclusion zone.
Ψ_r	Energy radiated by the mainshock.
Ψ_d	Energy dissipated by frictional sliding, plastic flow, etc., during the mainshock.
Ψ^{as}	Total energy radiated by aftershocks.
$\overline{M}$	Predicted maximum magnitude of any aftershock during the aftershock sequence.
$\sigma_{\text{eff}}\ (=\sigma_3 - P_f)$	Effective value of the local least principal stress.
P_f	Pore pressure within the focal volume of the primary inclusion zone.
$\eta\left(=\frac{\Psi_r}{\Psi_p}\right)$	Seismic efficiency factor.

Appendix B

An example of the dilatant or anomalous phase in rock is shown in Fig. B.1. This figure is a photograph of a corner section of an oil shale sample that illustrates the process of fault (F) growth. The initial length and diameter of this specimen were 10 cm and 5 cm, respectively. This specimen recovered nearly 10% of the total initial deformation ($\sim$0.25 cm) within one day following the test. Note the orientation of the deformation band (D), whose width is approximately one centimeter and the tensile cracks (t_0) that developed within the band in a direction nearly normal to the predicted direction of σ_1, that is, normal to the direction of eventual fault growth [6]. Microscopic examination of this deformation band, as well as other deformation bands within this specimen, shows the existence of numerous (apparently closed) small cracks (whose average lengths are approximately 0.01 cm) that are slightly inclined to the fault direction. Residual tensile and compressive stresses in the deformation band (following unloading) in directions parallel and normal to σ_1, respectively, are predicted by the inclusion theory [6]. The tensile strength of oil shale normal to the bedding plane is small ($\sim$50 bars, V. E. HOOKER, personal communication, 1975), and is suggestive that a major contributing factor to the post-test recovery of the specimen was the formation of the tensile cracks within the deformation band(s).

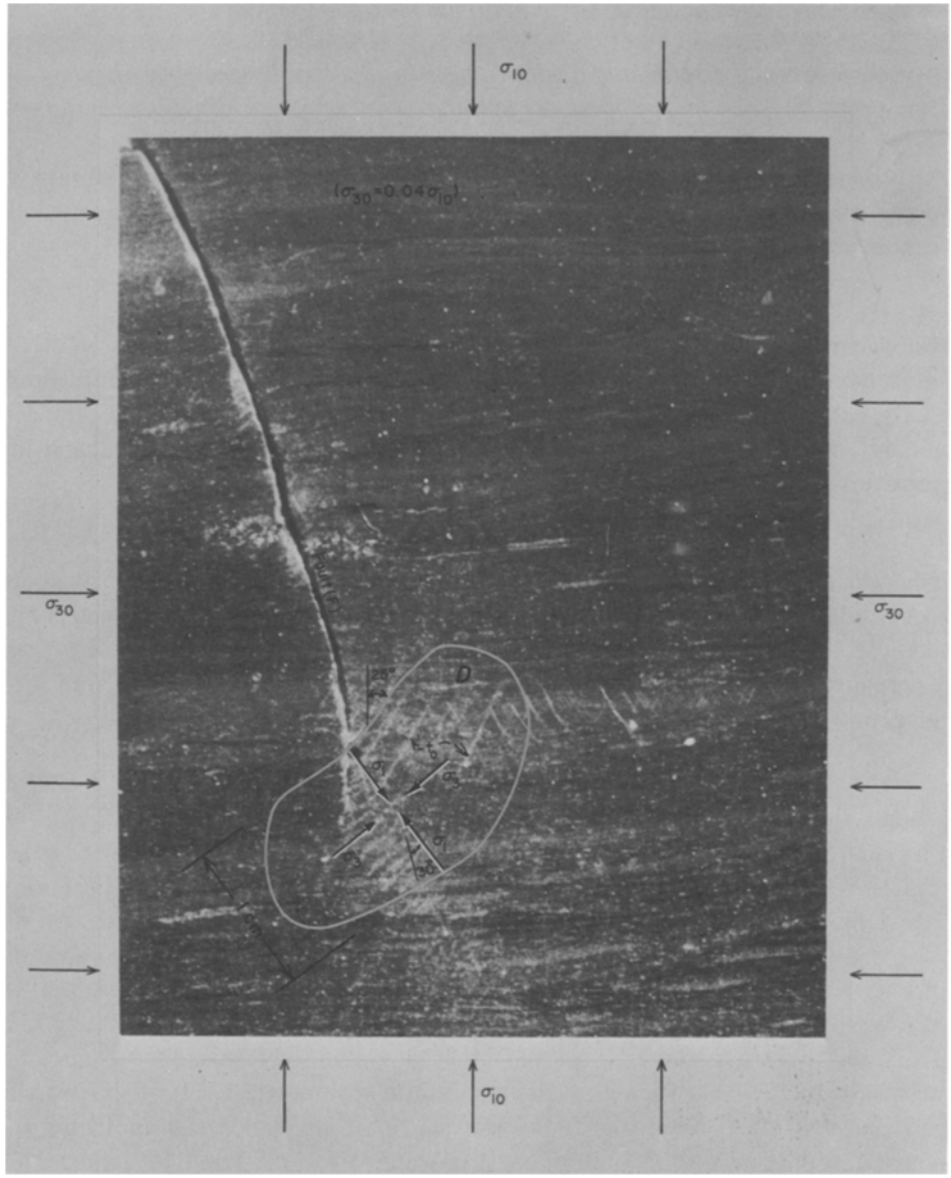

Figure B.1
Polished section of oil shale sample deformed under 100 bars confining pressure, illustrating the deformation band within which the fault developed.

Appendix C

Experimental determination of the precursor time–'fault' length relationship of failure

When there are *no* changes in the far-field tectonic stresses (strains) during the precursor time interval (τ), the relationship between τ and the focal region area (A) can be written [7]

$$\tau = \alpha A, \tag{C.1}$$

where α is a constant to be determined by experiment. Rockbursts, whose class I precursor times are small enough (≤ 24 hr) so to satisfy the constraints imposed by (C.1), can be used to evaluate the parameter α. Assume that the Utsu relationship (equation (7)) between magnitude (M) and aftershock area (A) is applicable to the rockburst failure. Equations (5) and (C.1) give

$$\log_{10} \tau_0 = 6.3 + \log_{10} \alpha + M, \tag{C.2}$$

where τ_0 is the class I precursor time and is measured in seconds. A major rockburst occurred in the Galena Mine, Wallace, Idaho, on 9 August 1968 (see reference 11 for details). The magnitude and precursor time of this burst were determined to be approximately $M2.3$ and 21.6 hr, respectively. Substituting these values into (C.2) gives $\alpha = 2.43 \times 10^{-4}$ sec/cm^2. Thus, equation (C.2) becomes

$$\tau_0 = 2.43 \times 10^{-4} A, \tag{C.3}$$

τ_0 and A are measured in seconds and square centimeters.

The relationship between the primary inclusion area (A_i) and A must be determined. A moderate rockburst occurred on 8 November 1975 (1:10 am) at the Galena Mine. Seismic data obtained from this burst allows a determination of the relationship of A_i and A as well as other critical parameters applicable to the scale invariant properties of the inclusion theory. Briefly, the following sequence of events preceded the burst. (1) Blasting in a nearby stope (mining zone), located approximately 75 m from the burst hypocenter, occurred at 2:23 pm on 7 November. No apparent seismic activity was triggered in the hypocentral region as a result of this blasting sequence. (2) At 11:20 pm on the same day, blasting occurred in another stope, located approximately 25 m from the hypocentral region. The time required for blasting was 8 min, during which time a length segment of approximately 15 m of rock was removed from the stope. (3) The burst occurred at 1:10 am, nearly 100 min after blasting.

Experimental studies by the Bureau of Mines in the Galena Mine have shown that the majority of rockbursts are apparently 'triggered' by blasting in stopes that are located in the immediate vicinity of the burst hypocenter. There are theoretical

arguments that support this observation. For example, using equations (C.1) and (C.3), the time τ_{d0}, required to form the primary inclusion zone of an impending burst is $\tau_{d0} = 2.43 \times 10^{-4} A_i$. Combining this relationship with the revised Utsu relationship ($\log A = M + 6.3$ [46])

$$\log_{10} \tau_{d0} = M + 2.69 + \log_{10} \mu \tag{C.4}$$

where $\mu = A_i/A$. The observed value of μ, as calculated from the 3 September 1975 Star burst is 0.046. Equation (C.4) becomes

$$\log_{10} \tau_{d0} = M + 1.35 \tag{C.5}$$

Thus, for a typical burst magnitude of $M1.5$, the time, τ_{d0}, required for the formation of the primary inclusion zone is nearly 6 min. However, the time required to form the individual seismic events whose magnitudes are of the order of $M(-3)$, that comprise the primary inclusion zone of an $M1.5$ burst are only a second. Therefore, the seismic signature of these events will be included within the signatures of the individual events. As a result, the primary inclusion zone of the impending burst will be formed by the stress transferrals to the critically stressed region (Fig. C.1) due to blasting. Consequently, the time interval required for blasting provides a maximal value of τ_{d0} (and A_i) for the impending burst.

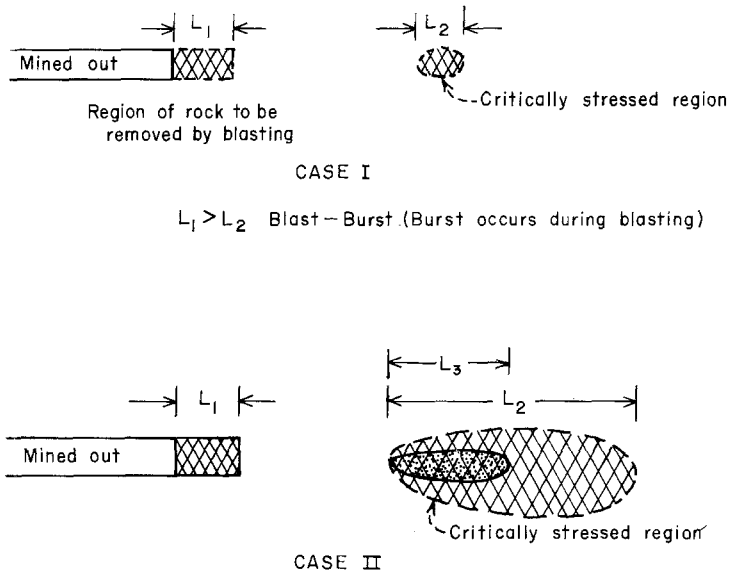

Figure C.1
Influence of blasting in triggering rockbursts. The critically stressed region represents the zone where the stresses have approached a critical state such that an increase in the maximum principal stress (resulting from blasting in a nearby region) will produce a burst.

The ratio of τ_{d0} (=8 min) and τ_0 (=100 min) for the 8 November 1974 burst gives a minimum estimate of τ_{d0}/τ_0 ($=A/A$) equal to 12.5. This value compares with the observed value of 21.8 calculated for the 3 September 1975 Star rockburst discussed earlier in the test.

Appendix D

Geometrical characteristics of the primary inclusion zone at the instant of failure

Theoretical and experimental arguments suggest that the length of the primary inclusion zone (L_i) and the average length (L_c) of the cracks that comprise this zone are proportional to each other with a proportionality constant, or equivalently, scaling factor γ ($=L_c/L_i$), experimentally observed to be approximately 0.01 (Appendix B). The scaling factor, γ, denotes the relationship by which the length (L_c) and thickness (t_c) of these cracks with respect to the length (L_i) and thickness (t_i), respectively, of the primary inclusion zone. Thus, the scaling law for the inclusion theory can be expressed as

$$L_c = \gamma L_i \qquad t_c = \gamma t_i \tag{D.1}$$

In the inclusion theory, failure, or equivalently, growth of the primary inclusion zone occurs only when the tensile stress within the primary inclusion zone equals its maximum possible value σ_{t0}. This physical situation develops only when the aspect ratio of the inclusion zone approaches a value that is of the order of 0.20 [8]. Several recent finite element investigations have shown that this aspect ratio is insensitive to the relative stiffness of the primary inclusion zone and the surrounding host material (BABCOCK, USBM, in press, 1976). Substituting this ratio in (D.1) gives

$$t_c = 2.0 \times 10^{-3} L_i \tag{D.2}$$

Thus, the condition for failure can also be stated that the ratio of the thickness of the crack zone to the length of the primary inclusion zone must equal approximately 2.0×10^{-3} at the instant of failure. This condition is also equivalent to the criterion that the tensile stress within the macrocrack zone becomes a maximum at failure.

To a first-order approximation, the crack zone thickness (t_c) will also equal the thickness of the macrocrack zone, say t_g, at the instant of failure. This thickness will also correspond to the thickness of the fault gouge zone. Consequently, when the focal region of the primary inclusion is circular ($A = (\pi/4)L^2$, $A_i = A/21.8$), the functional relationship between t_g and the class I precursor time τ_0 can be written

$$t_g = 0.03\sqrt{\tau_0} \tag{D.3}$$

where t_g and τ_0 are measured in centimeters and seconds, respectively.

Equation (D.3) predicts that a knowledge of the fault zone thickness along either active or inactive faults may be an indication of the magnitude of the earthquake(s) that produced the fault zone. The functional relationship of t_g to M, σ_3, and P_f is found from equations (5), (27), (28), and (D.3).

$$\log_{10} t_g = 0.50M + 0.66 \log_{10} \frac{\sigma_3 - P_f}{\sigma_3} - 0.18 \tag{D.4}$$

where M is the predicted magnitude of the mainshock when $P_f = 0$ and t_g is measured in centimeters.

Table D.1 lists the typical value of fault zone thickness for magnitudes ranging from $M(-)5$ to $M8$. The pore pressure is zero in these calculations. As an example,

Table D.1

Fault zone thickness–magnitude relationship
($P_f = 0$)

L_i km	L km	M	t_g km	Comments
1×10^{-5}	5×10^{-5}	−5	4.8×10^{-8}	Laboratory failure scale
1×10^{-3}	5×10^{-3}	−1	4.8×10^{-6}	Laboratory failure scale
1×10^{-3}	5×10^{-3}	1	4.8×10^{-5}	Mine failure scale
0.03	0.16	2	1.5×10^{-4}	Mine failure scale
0.10	0.5	3	4.8×10^{-4}	Mine failure scale
0.34	1.6	4	1.5×10^{-3}	Earthquake scale
1.1	5	5	4.8×10^{-3}	Earthquake scale
3.4	16	6	1.5×10^{-2}	Earthquake scale
10.6	50	7	4.8×10^{-2}	Earthquake scale
34	160	8	1.5×10^{-1}	Earthquake scale

a magnitude $M8$ earthquake corresponds to a fault zone thickness of nearly 60 m, while the thickness on the scale of major rock bursts ($M = 2 \rightarrow 3$) is only predicted to be in the range of $15 \rightarrow 48$ cm.

These values appear to be in good agreement with measurements taken in rock-burst prone mines in South Africa [17]. Also, note that t_g on the laboratory scale [$M(-)5$] is predicted to range in value from 10^{-3} cm, in reasonable agreement with measurements taken in our laboratory. Lastly, note that in real fault zones in the earth, where fluids under pressure are probably present, gouge zone thickness will be less than if the zone were 'dry' at the time of its formation.

If (D.4) is found by experiment to be applicable to real fault zones, it may become possible to predict the spacial distribution of earthquake magnitude along either active or inactive faults of known geologic age as a function of geologic time. Such a method may, in some instances, be of value in assessing seismic risk for engineering structures proposed or currently in operation in these regions.

The preceding calculations can be used to estimate the fault displacement that occurs during an earthquake of magnitude M. Let θ denote the angle between the major axis of the macrocrack zone (Fig. 1) and the maximum applied far-field principal stresses σ_{1_0}. In the inclusion theory of failure, the shear displacement that can occur during the mainshock sequence is due only to closure of the cracks that developed during the dilatant phase. These cracks formed under the applied far-field stresses, σ_{1_0}, σ_{2_0}, and σ_{3_0} (Fig. 2a). Thus, to a good first-order approximation, the total shear displacement, s_0, that will occur as the fault grows into the hypocentral region is

$$s_0 = t_g \cot \theta \tag{D.5}$$

As an example of (D.5), McGarr [17] observed that following a $M3$ rockburst, which produced violent crushing of supports in the vicinity of the burst, shear displacements of $30 \rightarrow 50$ cm were observed along the fault. Equation (D.4) gives $t_g = 48$ cm, where $P_f = 0$. The predicted relative shear displacement for a failure of this magnitude, assuming $\theta \approx 30°$, is 83 cm, in reasonable agreement with observation.

Lastly, it is important to observe that (D.1) suggests that the component of volumetric strain, ε ($\equiv \gamma$) due to the formation of the primary inclusion zone and its associated macrocrack zone at the *instant of failure* is approximately 1×10^{-2}. This result suggests that current theoretical methods of modeling shear dilatancy in rock by linear classical models may be unsatisfactory [21].